SRI International

Final Report • July 2018

Inverse-scattering Design of Metasurfaces

Final report covering the period 15 July 2017 through 14 July 2018

SRI Project P24564

Prepared by:

Brian Slovick, Principal Research Physicist
Srini Krishnamurthy, Senior Principal Scientist
Applied Optics Laboratory
Center for Security and Survivability
SRI International

Prepared for:

DARPA (DSO)
675 Randolph Street,
Arlington, VA 22203

Attn: Dr. Michael Fiddy, Program Manager

DISTRIBUTION STATEMENT A. Approved for public release. Distribution is unlimited.

1.0 TECHNICAL SUMMARY

This report on *Inverse-scattering Design of Metasurfaces* summarizes the work SRI International (SRI) has accomplished from 15 July 2017 through 14 July 2018 under DARPA contract HR001117C0118.

The primary objective of this program is to develop inverse-scattering methods to design *passive* metasurfaces for frequency conversion (FC). In particular, the goal is to extend the k-space formalism to study inelastic scattering from metasurfaces and explore the possibility of achieving FC using only linear materials by exploiting, for instance, the coupling between multiple resonances of metasurfaces and/or spatiotemporal modulation intrinsic in the materials.

Major achievements are:

1. Developed a formalism for studying direct and inverse scattering in dielectric media and applied k-space engineering approach to study both elastic and inelastic scattering.

2. Identified an approximation—called extended far-field approximation (EFA)—and demonstrated that it accurately predicts the scattered field even through resonance in high-index contrast structures.

3. Showed the EFA arrived at the closed form expression for inverse scattering studies both in elastic and inelastic cases. The ability to use closed-form expressions considerably speeds up the inverse-scattering studies.

4. Developed COMSOL-based codes to solve Maxwell equations with time-dependent permittivity and used them to verify the accuracy and validity of EFA.

5. Showed that both EFA and COMSOL codes predicted frequency conversion that was most effective when the resonance in metastructures was designed to be at the desired *scattered* frequency.

    a. This result is counterintuitive because the conventional understanding is that the resonant frequency must be matched to the incident frequency for the maximum scattering.

    b. This result opens up the design space for efficient linear frequency conversion as it alleviates the phase-matching requirement.

6. Identified passive systems with potential for time-dependent permittivity leading to FC.

2.0 TECHNICAL DISCUSSION

2.1 Background

The forward-scattering approach of electromagnetics specifies the permittivity distribution and solves Maxwell's equations to obtain the scattered fields. Alternatively, the inverse-scattering approach specifies the scattered fields and applies an inverse-scattering algorithm to calculate the permittivity distribution of the scattering source. The ability to use inverse-scattering methods to design structures with specific scattered fields would greatly benefit the development of metasurfaces—surfaces containing subwavelength structural elements designed to modify the amplitude and phase of the electromagnetic fields. The current state-of-the art (SOA) approach for designing metasurfaces relies on an iterative forward-scattering approach to design elements with the desired amplitude and phase in the scattered fields, resulting in inefficient design and suboptimal performance. A more promising approach is to employ inverse-scattering methods to directly calculate the size, shape, and permittivity of a scatterer from the specified amplitude and phase of the scattered fields.

The current project aims to develop inverse-scattering methods for designing metasurfaces. The main objective of the program is to develop an inverse-scattering formalism based on the Fourier (k)-space representation that can be used to design frequency-converting metasurfaces without using nonlinear materials. To achieve FC, we explored two approaches:

1. *Inelastic scattering metasurfaces*. Specified k-space diagram with incident and scattered wave vectors of different amplitudes and applied inverse-scattering methods to determine the associated permittivity distribution.

2. *Metasurfaces with spatiotemporally modulated permittivity*. Studied metasurfaces analogous to acousto-optic modulation in which the frequency shift of the scattered light is equal to the frequency at which the material is modulated. We explored both actively modulated metasurfaces and passive metasurfaces with self-induced permittivity modulation.

2.2 Results

Toward the eventual goal of studying frequency converting inelastic metasurfaces, first we developed the k-space formalism to study elastic scattering and then extended it to inelastic scattering.

2.2.1 Elastic scattering from time invariant media: In the time-invariant media, the dielectric function does not depend explicitly on time. For this case, we derived expressions for the scattering potential (dielectric function) from the scattered field in k-space as described in Appendix A. We then developed a MATLAB code that employed k-space formalism to calculate the dielectric function of the scatterer first using the Born approximation (Eq. A5), and then the Rytov approximation (Eq. A7). For validation, first we assumed an infinite cylinder of known radius and dielectric constant, and obtained the scattered fields for a wavelength of 1 μm using the full-wave frequency-domain solver HFSS. We then used the calculated field as input to our inverse scattering code to obtain the dielectric function. The results obtained in the first Born approximation are shown in Figure 1.

Note the dielectric function predicted from inverse scattering (middle and bottom row) agree with the assumed value of ε_r=1.2+0i only for the smallest radius value (R=0.1 μm). For larger radii, the inverse-scattering method yields real and imaginary parts of ε_r much larger than the assumed values. The Born approximation breaks down for larger cylinders. Similarly, we found (not shown) the first Born approximation also fails for cylinders with a larger dielectric constant in air. We also found the next level of approximation, the Rytov approximation, did not improve accuracy (not shown) in direct and inverse scattering.

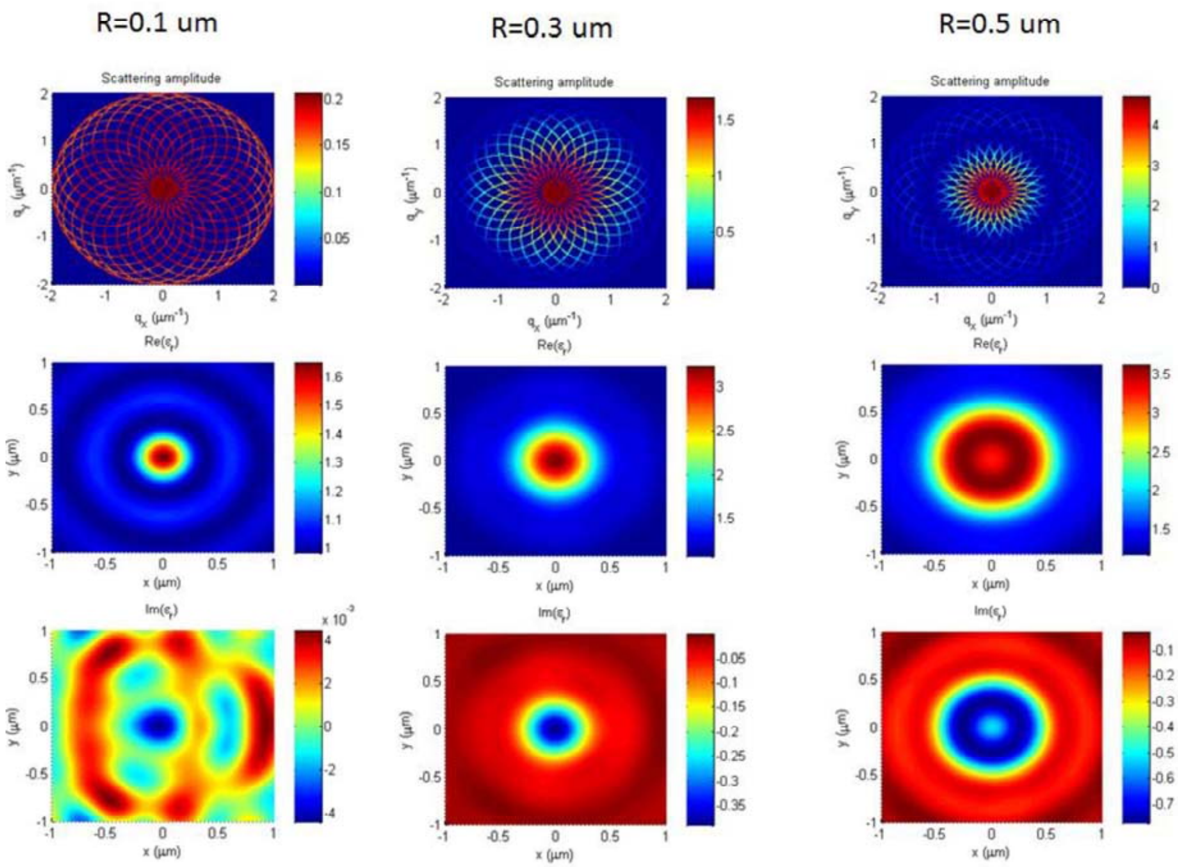

Figure 1: Inverse scattering with the Born approximation for cylinders (ε=1.2) with three different radii as noted for a wavelength of 1 μm. The calculated scattering amplitudes in k-space (top row), the real part of ε (middle row), and the imaginary part of ε (bottom row) are shown.

Extended far-field approximation (EFA): Our further analysis of the Green's function-based derivation indicated the infinite series can be non-perturbatively summed into a closed form when the angular dependence of scattered field within the scattering volume is the same as that in the far field. In the elastic-scattering case,

$$\begin{aligned} E_s\left(\boldsymbol{r},\mathbf{k_s},\mathbf{k_i}\right) &= \frac{e^{ikr}}{r} f_S\left(\theta,\phi,\omega\right) \\ f_S\left(\theta,\phi,\omega\right) &= f_S\left(\theta',\phi',\omega\right) \end{aligned} \tag{1}$$

where E_s is the scattered electric field, f_s is the scattering amplitude, k_i and k_S denote the incident and scattered wave vectors, and the primes denote the angular values inside the scatterer. This approximation—called EFA—enables us to obtain analytical solutions to both scattered field and the dielectric function as described in detail in Appendix B.

We then numerically verified the accuracy of the approximation by considering both 2D and 3D structures, spherically symmetric and asymmetric structures, and increasing the dielectric contrast (between the structure and the background). Interestingly, the accuracy was found be valid even through Mie resonance for all cases considered as long as the dielectric contrast was about 8. Since none of the closed-form expression available in the literature is accurate near resonance in high-contrast structures, we summarized the results and submitted a paper to

Physical Review Letters for possible publication. The results of the test performed and the applicability and the limitations of the EFA are discussed in detail in the manuscript, which is included here as Appendix C.

2.2.2 Inelastic scattering from time-variant media: As we have seen, in time-invariant media in which the dielectric function is time-independent, the FC does not occur. To arrive the conditions for the FC, we began with most general Maxwell equations in which the dielectric is also time-dependent and shows, as described in Appendix D, that the FC is possible only when susceptibility has intrinsic or extrinsic time dependence. This formalism is then extended to apply EFA.

Briefly, for inelastic scattering, the permittivity ε(or equivalently susceptibility χ) will have extrinsic time dependence and the Maxwell equation is:

$$\left(\nabla^2 - \frac{1}{c^2}\frac{\partial^2}{\partial t^2}\right)\mathbf{E}(\mathbf{r},t) = \frac{1}{c^2}\frac{\partial^2}{\partial t^2}\left[\chi(t)\mathbf{E}(\mathbf{r},t)\right] \tag{2}$$

The Fourier transform of the above equation reduces to:

$$\left(\nabla^2 + k^2\right)\mathbf{E}(\mathbf{r},\omega) = -4\pi\left[\frac{k^2}{4\pi}\int_{-\infty}^{\infty} d\Omega\,\chi(\Omega)\mathbf{E}(\mathbf{r},\omega-\Omega)\right] \tag{3}$$

where k=ω/c. The corresponding Green's function equation is:

$$\left(\nabla^2 + k^2\right)G(\mathbf{r},\mathbf{r}',\omega) = -4\pi\delta(\mathbf{r}-\mathbf{r}') \tag{4}$$

and the solution to Eq. 3 in terms of G is, as before in far field approximation is:

$$\begin{aligned}\mathbf{E}(\mathbf{r},\omega) &= -\frac{1}{4\pi}k^2\int d^3r'\,\frac{e^{ik|\mathbf{r}-\mathbf{r}'|}}{|\mathbf{r}-\mathbf{r}'|}\int_{-\infty}^{\infty} d\Omega\,\chi(r',\Omega)\mathbf{E}(\mathbf{r}',\omega-\Omega)\\ &\approx -\frac{1}{4\pi}k^2\frac{e^{ikr}}{r}\int d^3r'\,e^{ik_s\cdot r'}\int_{-\infty}^{\infty} d\Omega\,\chi(r',\Omega)\mathbf{E}(\mathbf{r}',\omega-\Omega)\end{aligned} \tag{5}$$

The total field is the sum of incident field at ω_i and scattered field. Thus,

$$\mathbf{E}(\mathbf{r},\omega'') = E_i(r,\omega'')\delta(\omega''-\omega_i) + E_S(r,\omega'') \tag{6}$$

Substituting Eq. 6 in Eq. 5, we get:

$$\begin{aligned}\mathbf{E}_S(\mathbf{r},\omega) &= -\frac{1}{4\pi}k^2\frac{e^{ikr}}{r}\int d^3r'\,e^{-ik_s\cdot r'}\int_{-\infty}^{\infty} d\Omega\,\chi(r',\Omega)\mathbf{E}_i(\mathbf{r}',\omega-\Omega)\delta(\omega-\Omega-\omega_i)\\ &\quad -\frac{1}{4\pi}k^2\frac{e^{ikr}}{r}\int d^3r'\,e^{-ik_s\cdot r'}\int_{-\infty}^{\infty} d\Omega\,\chi(r',\Omega)\mathbf{E}_S(\mathbf{r}',\omega-\Omega)\\ &= -\frac{1}{4\pi}k^2\frac{e^{ikr}}{r}\int d^3r'\,e^{-ik_s\cdot r'}\,\chi(r',\omega-\omega_i)e^{ik_i\cdot r'}\\ &\quad -\frac{1}{4\pi}k^2\frac{e^{ikr}}{r}\int d^3r'\,e^{-ik_s\cdot r'}\int_{-\infty}^{\infty} d\omega'\,\chi(r',\Omega)\mathbf{E}_S(\mathbf{r}',\omega-\Omega)\end{aligned} \tag{7}$$

If we assume $\Omega << \omega$,—that is the shift in the frequency is much smaller than the interrogating frequency—then the EFA can be applied as before. Using Eq. 1 we get<

$$\mathbf{E}_S(\mathbf{r},\omega) = -\frac{1}{4\pi}k^2\frac{e^{ikr}}{r}\int d^3r'\, e^{-iq\cdot r'}\,\chi(r',\omega-\omega_i)$$
$$-\frac{1}{4\pi}k^2\frac{e^{ikr}}{r}\int d^3r'\, e^{-ik_s\cdot r'}\int_{-\infty}^{\infty} d\Omega\,\chi(r',\Omega)\,\frac{e^{i\bar{k}r'}}{r'}f_S(\theta',\phi',\omega) \tag{8}$$

$$\Rightarrow \mathbf{E}_S(\mathbf{r},\omega) = \frac{-\frac{1}{4\pi}k^2\frac{e^{ikr}}{r}\int d^3r'\, e^{-iq\cdot r'}\,\chi(r',\omega-\omega_i)}{1+\frac{1}{4\pi}k^2\int d^3r'\, e^{-ik_s\cdot r'}\int_{-\infty}^{\infty} d\Omega\,\chi(r',\Omega)\frac{e^{i\bar{k}r'}}{r'}}$$

This expression is similar to the elastic-scattering case. The Eq. (8) can be inverted to obtain $\chi(r,\Omega)$ in terms of $E_s(r,\omega)$ as in the case of elastic-scattering studies.

First, we used EFA to calculate the scattering cross section, both elastic and inelastic, for infinitely long cylinders subjected to time harmonic (i.e., single frequency) modulations (Figure 2). The required equations for cylinders are given in Appendix E. For these calculations, the incident frequency is 30 THz, ε_r=8, and the modulation amplitude is δ=0.1. We calculated the cross sections, normalized to the cross-sectional area of the cylinder, for modulation frequencies of 5 THz (left), 10 THz (middle), and 20 THz (right). The top panel shows the cross section for elastic scattering, i.e., scattering at 30 THz. In this case, the cross section is a maximum for a particle radius of 0.64 μm. The bottom panels show the cross section for the sum and difference frequencies. Interestingly, we found the particle size needed to maximize inelastic scattering differed from the value needed to maximize elastic scattering, and in addition, was different for

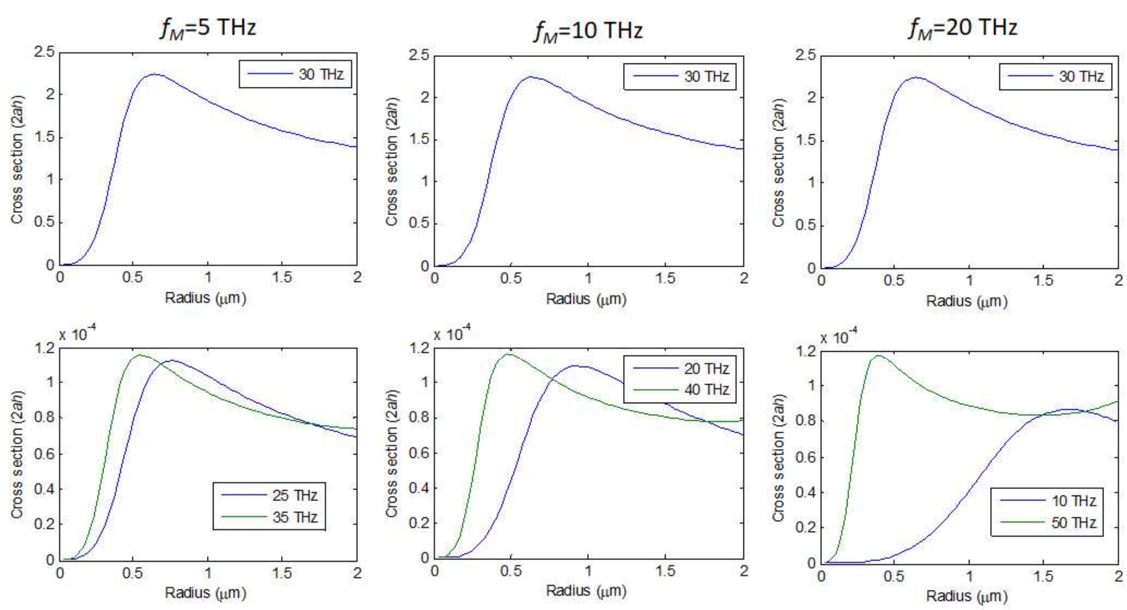

Figure 2. Calculated scattering cross section for infinitely long cylinders subjected to time-harmonic modulations of 5 THz (left), 10 THz (middle), and 20 THz (right), as a function of radius. The top plot shows the results for elastic scattering at 30 THz, while the bottom plot shows the cross section for the inelastic scattered fields.

the sum and difference frequencies. In fact, when the results were plotted as a function of $k_j a$, where k_j is the relevant wavenumber, all resonances occurred at the same value, implying the particle size for maximum scattering is inversely proportional to the value of k_j, or equivalently, directly proportional to the wavelength as shown in Figure 3.

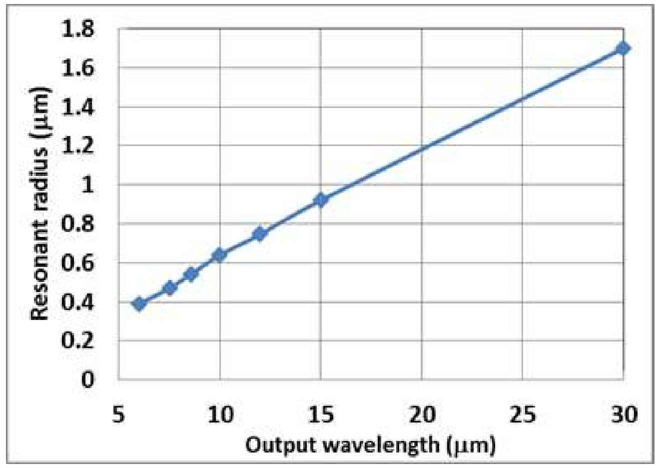

Figure 3: The variation of resonant radius with the wavelength of scattered waves.

One of the important conclusions from these calculations is that the scattering is largest when the meta-element has resonance at the *scattered* frequency. In traditional Mie-scattering-based metasurface design for elastic scattering, the resonant frequency is chosen to be the incident frequency. The calculations indicate that for inelastic scattering and maximum conversion, the elements have to be resonant at the output frequency. This observation has strong implications. Linear frequency conversion approaches, as discussed in the following section, can be designed for efficient conversion by eliminating the need for complicated phase matching. Since the conclusion is valid independent of how the photons are generated inside the scatterer, this is applicable for absorbing and re-emitting (at lower frequency) structures as well. In addition to FC metasurfaces, we see this principle can be used in designing up-/down- converting particle sizes for enhanced brightness of selective colors in a display.

We also developed full-wave time-domain COMSOL codes to calculate the inelastic scattering by infinitely long cylinders subjected to time-harmonic modulations. These simulations confirm the results obtained with EFA described above, though convergence issues made it difficult to make quantitative comparisons.

3.0 Linear FC options

Starting from the time-dependent linear wave equation, we identified the conditions for FC. We showed that FC is possible as long as the permittivity is also time-dependent at the time of illumination. This occurs when the permittivity is

a. Time-dependent even for a short time during illumination,

b. Modulated in time by mechanisms intrinsic to the material, for example by phonons,

c. Modulated externally, for example by voltage.

Since we are interested in passive and linear FC systems, option *c* was not considered further. We explored possible systems in categories *a* and *b* above. Based on the above calculations and a literature survey on metasurfaces for FC, we identified a few systems and requirements for passive linear conversion.

Dipoles and Raman Solids: Let us consider two dipoles in close proximity. When one of the dipoles is excited by incident radiation, the oscillating charges produce an oscillating electric field at the other dipole. The charges in the second dipole will start oscillating, which in turn will produce an oscillating electric field. In this mechanism, known as Forster resonance energy transfer (FRET), the energy from the incident radiation is transferred non-radiatively through the

Coulomb interaction (or by virtual photons). When the incident frequency is matched to the resonant frequency of the dipole, the scattering is most efficient. However, even if the resonant frequencies of the dipoles are different, the frequency of the scattered wave will be identical to that of the incident wave, because the frequency of the second dipole is initiated and sustained by that of the incident radiation (and first dipole). As such, there will be no FC. Similarly, two meta-atoms or meta-molecules, which behave like dipoles at their lowest-order resonances, can transfer energy non-radiatively, but the frequency of the scattered radiation will not change.

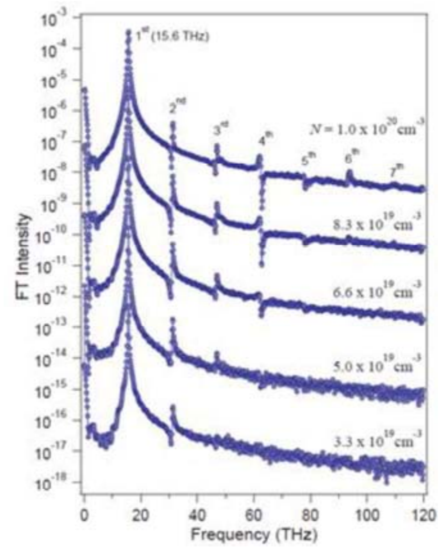

Figure 4: Output frequencies are shifted from the incident frequencies by the multiples of fundamental longitudinal optical (LO) phonon frequency of 15.6 THz in doped Si.

On the other hand, FC may occur if the dipoles oscillate independently of the incident radiation. Examples include Raman scattering by vibrating molecules and Brillouin scattering by acoustic phonons in passive systems. For passive FC to use materials or system in which permittivity has intrinsic or inherent time dependence, one such possibility is to exploit Raman scattering. The lattice oscillations—particularly the longitudinal optical phonons—have stronger interactions with photon field by way of electrons in the system. For example, FC has been demonstrated in doped Si (and GaAs) for frequency close to the direct gap of Si, as shown in Figure 4 [Hase et al., New J. of Phys., **15**, 055018 (2013)].

Fluorescent materials: The presence of concentrated electric fields at the dipole site change the local environment (i.e., the bonding arrangement in the excited state or local polarization). One example is fluorescent materials in which the emission and absorption spectrum are shifted in frequency even at low intensities. Notice that in both dipole and fluorescent cases, the local permittivity evolves in time independently from the incident field, which is a requirement for FC. In fluorescent materials, the incident radiation induces a step-function-like change in the permittivity with time.

External Triggers: There are several publications that describe FC. The methods employ external triggers to change the permittivity (a) between interacting meta-elements shown in Fig. 5a [Lee et al, https://www.researchgate.net/publication/317344130], (b) of elements on the surface surrounding high Q cavity shown in Fig. 5b [Notomi and Mitsugi, Phys. Rev. A73, 051803 (2006)], or (c) by an impulse as the wave-front progresses through the material as shown in Fig. 5c [Xaio and Agrawal, https://doi.org/10.1364/FIO.2010.FWQ5]. At low intensities, FC has been demonstrated in a design that employs hyperbolic metamaterial to enhance the interaction between the fluorescent material (R6G and Alq3) with overlapping absorption and emission spectrum (Fig. 5d). [Newman et al., https://doi.org/10.1364/CLEO_QELS.2015.FM3C.1].

We will consider the following options for designing passive metasurfaces for FC:

Fluorescent materials: Design a non-absorbing meta-element whose resonant frequency is close to the incident frequency. Choose a fluorescent material such as R6G whose absorption spectrum includes the designed resonant frequency and places it in close proximity to the resonator. When

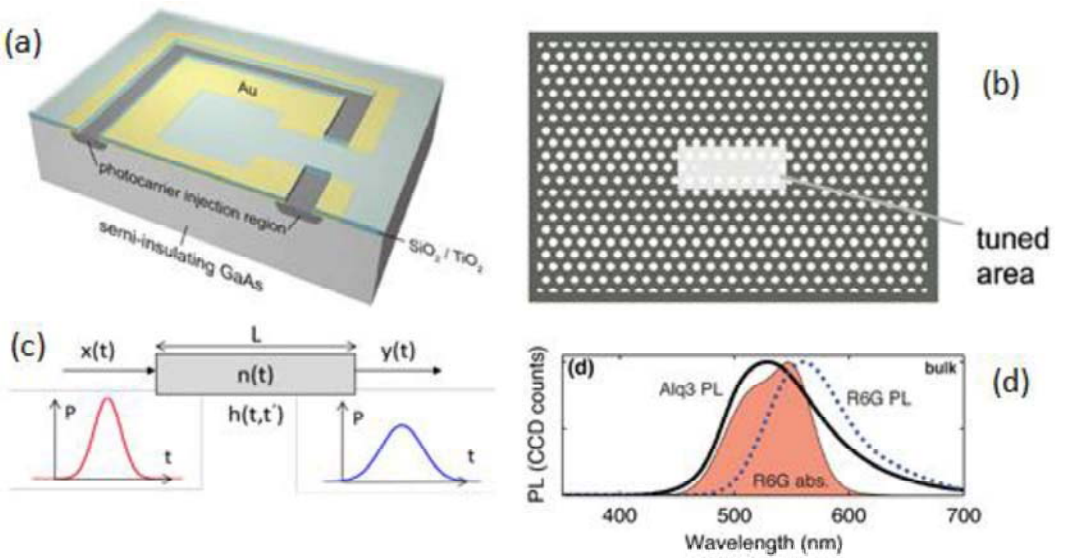

Figure 5: Some of the predicted or demonstrated designs for linear frequency conversion. (a) The intermediate region between two C-rings is photo-excited. (b) Meta-atoms around the defect in photonic crystals are photo activated. (c) There is an impulse change to refractive index. (d) The difference between emission and absorption frequencies of R6G is exploited for frequency conversion. All except (d) require external activation.

the radiation is incident on resonator, it will transfer energy non-radiatively to R6G, which in turn will emit at frequencies different from the incident frequency. Since the emission will be isotropic, the resonator-R6G pair will be placed in an array specifically chosen to radiate in one direction in the far field.

(a) <u>Cavity:</u> Include elements near the cavity that are replaced or coated with fluorescent material. This is a slightly modified version of design (a) above. The permittivity change induced by the incident field may be large enough to shift the emission frequency.

(b) <u>Raman:</u> Choose an incident frequency ω_0 and material with a sizable longitudinal optical (LO) phonon frequency. Identify the frequency, ω_{LO}, near which the LO Raman modes are active. Design a meta-element made of that material to resonate at that $\omega_0 + \omega_{LO}$ or $\omega_0 - \omega_{LO}$ frequency. Because of photon-phonon coupling, the frequency of some portion of the emitted light will be shifted. The energy transfer is most efficient when the element's resonant frequency matches the scattered frequency. Since the emission will be in all directions, the resonator will be placed in an array specifically chosen to radiate in one direction in the far field.

(c) <u>Three-level systems</u>: Consider a material or design with a three-level system as shown in Figure 6. The incident photon with energy E_{13} is absorbed, resulting in an electron from L1 being promoted to L3. The electron decays quickly to L2 by nonradiative process and eventually recombines with holes in L1, emitting a down-converted photon with energy E_{12}. If the element made of this material is designed to have E_{23} to be one LO photon energy and to have resonant frequency at $E_{12}/\hbar$, a most efficient, passive, and linear

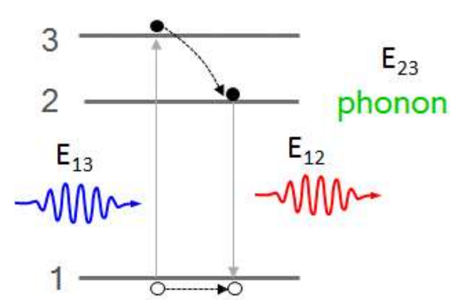

Figure 6: Three-level system converts incident photon with energy E_{13} to output photons with energy E_{12}.

frequency conversion can be expected. Note the design is not limited to materials with three-level systems

4.0 Conclusions

In summary, we have studied both elastic and inelastic scattering by solving Maxwell equations with a new approximation—extended far-field approximation—and obtained closed-form expression for scattered field and permittivity profile of the scatterer. The EFA has been tested and produced accurate results for permittivity contrast of 8. The ability to use closed-form expressions considerably speeds up the inverse-scattering studies. Our calculations indicate that FC is possible as long as the permittivity is also time dependent at the time of illumination. The time dependence can be intrinsic as in Raman solids and fluorescent materials, or extrinsic as in voltage or acoustic-controlled solids, or it can be designed to have absorption and multiple energy levels with energy transfer assisted by radiative or nonradiative process. Importantly, we conclude that meta-elements need to be designed to have resonance at the scattered frequency for more efficient frequency conversion. We have identified a few likely designs for passive and linear frequency conversion.

APPENDIX A:
INFINITE BORN SERIES

The scalar wave equation for time-invariant media is:

$$\left(\nabla^2 - \frac{1}{c^2}\frac{\partial^2}{\partial t^2}\right)\psi(\mathbf{r},t) = \frac{1}{c^2}\frac{\partial^2}{\partial t^2}\left([\varepsilon(r)-1]\psi(\mathbf{r},t)\right). \tag{A1}$$

Taking the Fourier transform of Eq. (A1), we obtain:

$$\begin{aligned}\left(\nabla^2 + k^2\right)\psi(\mathbf{r},\omega) &= -4\pi\left[\frac{k^2\left(\varepsilon(r)-1\right)}{4\pi}\right]\psi(\mathbf{r},\omega)\\ &\equiv -4\pi V(r)\psi(\mathbf{r},\omega)\end{aligned} \tag{A2}$$

where $k=\omega/c$. Noting that the Green's function $G(r,r')$ is the solution of:

$$\left(\nabla^2 + k^2\right)G(|\mathbf{r}-\mathbf{r}'|) = -4\pi\,\delta(|\mathbf{r}-\mathbf{r}'|), \tag{A3}$$

the general solution for the total field is:

$$\psi(\mathbf{r},\omega) = \psi_i(\mathbf{r},\omega) + \int d^3r'\; G(|\mathbf{r}-\mathbf{r}'|)V(r')\psi(\mathbf{r}',\omega), \tag{A4}$$

where ψ_i is the incident field. In the inverse scattering approach, $V(r)$ is calculated from the known incident field and the scattered field specified in the far field. However, the integral in Eq. A4 is over the region within the scattering element where the scattering potential is non-zero and the field is unknown. Hence $V(r)$ can only be obtained approximately. In the most common approximation—called first Born approximation— the total field $\psi(\mathbf{r},\omega)$ inside the scattering element is replaced by $\psi_i(\mathbf{r},\omega)$. In the far field approximation, r>>r' and

$$\begin{aligned}|\mathbf{r}-\mathbf{r}'| &= \left[r^2 + r'^2 - 2\,\mathbf{r}\cdot\mathbf{r}'\right]^{1/2}\\ &\approx r - \frac{\mathbf{r}}{r}\cdot\mathbf{r}'\\ &= r - \frac{\mathbf{k_s}}{k}\cdot\mathbf{r}'\end{aligned}$$

and the Green's function is simplified as

$$\begin{aligned}G(|r-r'|) &= \frac{e^{ik|r-r'|}}{|r-r'|}\\ &= \frac{e^{ikr}}{r}e^{-i\mathbf{k_s}\cdot\mathbf{r}}\end{aligned}$$

In the Born approximation, the ψ inside the integral in Eq. 4 is replaced by the incident wave, $e^{i\mathbf{k}_i\cdot\mathbf{r}}$ we have:

$$\psi(\mathbf{r},\omega) \simeq \psi_i(\mathbf{r},\omega) + \frac{e^{ikr}}{r}\int d^3r'\; V(r')e^{-i(\mathbf{k}_s-\mathbf{k}_i)\cdot\mathbf{r}'} \tag{A5}$$

But, from full calculations, the ψ can be written as a sum of incident wave and scattered wave in the form:

$$\psi(\mathbf{r},\omega) = \psi_i(\mathbf{r},\omega) + \frac{e^{ikr}}{r} f(\mathbf{k}_s - \mathbf{k}_i, \omega)$$
$$f(\mathbf{k}_s - \mathbf{k}_i, \omega) = \int d^3r'\, V(r') e^{-i(\mathbf{k}_s - \mathbf{k}_i)\cdot\mathbf{r}'} \equiv \int d^3r'\, V(r') e^{-i\mathbf{q}\cdot\mathbf{r}'} \tag{A6}$$

Taking the Fourier transform of both sides with respect to **q** we obtain:

$$V(r) = \int d^3q\ f(\mathbf{q},\omega) e^{i\mathbf{q}\cdot\mathbf{r}} \tag{A7}$$

The scattering amplitude $f(\mathbf{q},\omega)$ is obtained for various incident and scattered wave vectors from either measurements or full-wave solutions to Maxwell's equations.

The Born approximation appears to work well away from resonance, i.e., for small scatterers and low-permittivity contrast. The other common approximation—Rytov approximation—works better for sizes larger than resonant sizes and higher contrast. In this approximation, a complex phase shift is added to the incident; when it is substituted in the wave equation one obtains:

$$\psi_i(\mathbf{r},\omega) \ln\left[\frac{\psi(\mathbf{r},\omega)}{\psi_i(\mathbf{r},\omega)}\right] = \frac{e^{ikr}}{r} \int d^3r'\, V(r') e^{-i\mathbf{q}\cdot\mathbf{r}'} \tag{A8}$$

We see that Eq. A8 is similar to Eq. A6, except the expression in the left-hand side of the equation is slightly more complicated, but can be evaluated.

APPENDIX B:
EXTENDED FAR-FIELD APPROXIMATION (EFA): ELASTIC SCATTERING

Since both Born and Rytov approximations are invalid near resonance, we return to Eq. (A4) to carry out the infinite series in a form suitable for inverse scattering studies. We recast Eq. (A4) by considering that total field is a sum of incident (i) and scattered (s) fields. We get,

$$\psi_S(\mathbf{r},\omega) = \int d^3r' G(|\mathbf{r}-\mathbf{r}'|)V(r')\left[\psi_i(\mathbf{r}',\omega)+\psi_S(\mathbf{r}',\omega)\right] \tag{B1}$$

In the far-field approximation, the Green's function takes the form,

$$\begin{aligned} G(|r-r'|) &= \frac{e^{ik|r-r'|}}{|r-r'|} \\ &= \frac{e^{ikr}}{r} e^{-i\mathbf{k_s}\cdot\mathbf{r}} \end{aligned} \tag{B2}$$

Substituting Eq. (B2) in Eq. (B1), we get:

$$\psi_S(\mathbf{r},\omega) = \frac{e^{ikr}}{r}\int d^3r' e^{-i\mathbf{k}_s\cdot\mathbf{r}'}V(r')e^{i\mathbf{k}_i\cdot\mathbf{r}'} + \frac{e^{ikr}}{r}\int d^3r' e^{-i\mathbf{k}_s\cdot\mathbf{r}'}V(r')\psi_S(\mathbf{r}',\omega) \tag{B3}$$

In the extended far-field approximation (EFA), we assume the angular distribution of the field inside the scatterer is the same as that in the far field. In other words,

$$\begin{aligned} \psi_s(\boldsymbol{r},\omega) &= \frac{e^{ikr}}{r} f_S(\theta,\phi,\omega) \\ f_S(\theta,\phi,\omega) &= f_S(\theta',\phi',\omega) \end{aligned} \tag{B4}$$

Substituting Eq. (B4) in B3, we get,

$$\begin{aligned} \psi_S(\mathbf{r},\omega) &= \frac{e^{ikr}}{r}\int d^3r' e^{-i\mathbf{k}_s\cdot\mathbf{r}'}V(r')e^{i\mathbf{k}_i\cdot\mathbf{r}'} + \frac{e^{ikr}}{r}\int d^3r' e^{-i\mathbf{k}_s\cdot\mathbf{r}'}V(r')\frac{e^{ikr'}}{r'} f_S(\theta',\phi',\omega) \\ &= \frac{e^{ikr}}{r}\int d^3r' e^{-i(\mathbf{k}_s-\mathbf{k}_i)\cdot\mathbf{r}'}V(r') + \frac{e^{ikr}}{r} f_S(\theta,\phi,\omega)\int d^3r' e^{-i\mathbf{k}_s\cdot\mathbf{r}'}V(r')\frac{e^{ikr'}}{r'} \\ &= \frac{e^{ikr}}{r}\int d^3r' e^{-i(\mathbf{k}_s-\mathbf{k}_i)\cdot\mathbf{r}'}V(r') + \psi_S(\mathbf{r},\omega)\int d^3r' e^{-i\mathbf{k}_s\cdot\mathbf{r}'}V(r')\frac{e^{ikr'}}{r'} \end{aligned} \tag{B5}$$

We see the first term on the right-hand side (RHS) is simply the Born term and the second term can be moved to the left-hand side (LHS) to get a closed for expression for the scattered field as:

$$\psi_S(\mathbf{r},\omega) = \frac{\frac{e^{ikr}}{r}\int d^3r' V(r')e^{-i(\mathbf{k}_s-\mathbf{k}_i)\cdot\mathbf{r}'}}{1-\int d^3r'' e^{-i\mathbf{k}_s\cdot\mathbf{r}''}V(r'')\frac{e^{ikr''}}{r''}} \tag{B6}$$

Notice that Eq. 12 has a similar form to the first Born expression except for a $\mathbf{k}_S$-, or angle-dependent denominator arising from the infinite series sum. In terms of the scattering amplitude, Eq. (B6) can be written as:

$$f(\mathbf{q},\omega) = \frac{\int d^3r' V(r')e^{-i\mathbf{q}\cdot\mathbf{r}'}}{1-\int d^3r'' e^{-i\mathbf{k}_s\cdot\mathbf{r}''}V(r'')\frac{e^{ikr''}}{r''}} \tag{B7}$$

The Eq. (B7) gives the scattering amplitude as a function of the potential, accurate to all orders. In the forward scattering problem, $V(r)$ is known and the scattering amplitude $f(\mathbf{q},\omega)$ can be determined from Eq. (B7). In the inverse scattering problem, $f(\mathbf{q},\omega)$ is known and $V(r)$ needs to be obtained. Taking the Fourier transform (FT) of Eq. (B7) with respect to $\mathbf{q}$, we obtain:

$$\int d^3q e^{i\mathbf{q}\cdot\mathbf{r}} f(\mathbf{q},\omega) \equiv V_B(r) = \frac{V(r)}{1-\int d^3r' e^{-i\mathbf{k}_s\cdot\mathbf{r}'} V(r') \frac{e^{ikr'}}{r'}}, \tag{B8}$$

where $V_B(r)$ is the potential obtained from the first Born approximation. Rearranging Eq. (B8):

$$V(r) = V_B(r)\left[1-\int d^3r' e^{-i\mathbf{k}_s\cdot\mathbf{r}'} V(r') \frac{e^{ikr'}}{r'}\right] \tag{B9}$$

Substituting this expression for $V(r')$ in the integral,

$$V(r) = V_B(r)\left[1-\int d^3r' e^{-i\mathbf{k}_s\cdot\mathbf{r}'} \frac{e^{ikr'}}{r'} V_B(r')\left(1-\int d^3r'' e^{-i\mathbf{k}_s\cdot\mathbf{r}''} \frac{e^{ikr''}}{r''} V_B(r'')\right)+\ldots\right] \tag{B10}$$

Equation (B10) can be summed in a geometric series to obtain,

$$V(r) = \frac{V_B(r)}{1+\int d^3r' e^{-i\mathbf{k}_s\cdot\mathbf{r}'} \frac{e^{ikr'}}{r'} V_B(r')} \tag{B11}$$

Equation (B11) gives the potential in terms of the first Born potential V_B, which is the FT of the scattering amplitude $f(\mathbf{q})$ by Eq. (B7), and is accurate to all orders. For the geometric series to converge, this summation implicitly assumes the integral in the denominator is small and needs to be verified in all calculations.

APPENDIX C:
MANUSCRIPT SUBMITTED TO *PHYSICAL REVIEW LETTERS*

Nonperturbative solution to the scattering problem

Brian Slovick* and Srini Krishnamurthy
Applied Optics Laboratory, SRI International, Menlo Park, California 94025, United States

We obtain a nonperturbative, analytical solution to the Lippman-Schwinger scattering equation by assuming the field within the scattering object is a spherical wave with a scattering amplitude equal to that of the far field. This approach is generally applicable to electromagnetic, acoustic, and quantum mechanical scattering, though here we apply it to classical electromagnetic scattering. First, we show this approximation is valid for both spherical and non-spherical objects, and that the calculated scattering cross section is accurate through the fundamental resonance frequency. Then we apply our general analytical expression to the inverse scattering problem and show that accurate reconstructions of the object are possible even under resonance conditions. The simplicity, generality, and accuracy of our method suggest it can be a reliable and efficient tool for understanding a wide range of scattering problems in physics.

Direct and inverse scattering problems are prevalent throughout physics [1–6]. In the direct scattering problem, the properties of the object are used to determine the scattered fields, a scenario routinely encountered in particle physics [7, 8], acoustics [9], and electromagnetics [3, 10]. In the inverse scattering problem [5, 10–12], the properties of the object are determined from the scattered fields. Inverse scattering is important for applications such as remote sensing [13–15], medical imaging [16, 17], and design and optimization of complex materials [18–22]. A general analytical solution to the direct and inverse scattering problem would benefit these fields and applications by providing provide new physical insight and more efficient computation.

The predominant methods for solving the scattering problem are partial wave analysis [1, 23], the Born approximation [7, 9, 24, 25], and numerical methods [1, 12, 26]. All have their advantages and limitations. Partial wave analysis is exact, but is limited to objects with rotational symmetry and cannot be used to solve the inverse scattering problem because the equations are transcendental [1, 10]. The Born approximation provides a closed-form expression and is valid for all object shapes [9, 27], but is limited to weak scattering conditions [24, 25, 28]. Numerical methods are exact within numerical error, but provide limited physical insight and are inefficient due to the difficulty of solving integral equations [1, 12, 26].

In this Letter, we obtain a nonperturbative closed-form solution to the Lippman-Schwinger (LS) scattering equation using what we call the extended far-field approximation (EFA), which generally applies to quantum mechanics, electromagnetics, and acoustics. The EFA is based on our empirical observation that the field within the object has the same scattering amplitude as the far-field scattering amplitude. Using full-wave simulations, we show the EFA is valid well into the scattering volume for spherical and non-spherical shapes, and that the scattering cross section for spheres obtained with EFA agrees well with exact calculations obtained by partial wave analysis, even through the first resonance. In addition, assuming convergence of an infinite geometric series, our closed-form expression can be inverted to obtain the potential in terms of the scattered field. Within the limits of this approximation, the EFA provides much improved inverse scattering reconstructions compared to the Born approximation. The simplicity and accuracy of our method suggest it can be a reliable and efficient tool for understanding scattering problems throughout physics.

Our closed-form expression can be derived from the inhomogeneous wave equation for a time-harmonic scalar field $U(\mathbf{r},\omega)$ [23, 27],

$$(\nabla^2 + k^2)U(\mathbf{r},\omega) = -4\pi F(\mathbf{r},\omega)U(\mathbf{r},\omega), \qquad (1)$$

where $F(\mathbf{r},\omega)$ is the scattering potential and k is the wavenumber. With the Sommerfeld radiation condition, the solution to Eq. (1) is given by the sum of the incident field $U_i(\mathbf{r},\omega)$ and the scattered field, given by [23, 27]

$$U_s(\mathbf{r},\omega) = \int d^3r' G(\mathbf{r}-\mathbf{r}',\omega)F(\mathbf{r}',\omega)[U_i(\mathbf{r}',\omega)+U_s(\mathbf{r}',\omega)], \qquad (2)$$

where the Green's function

$$G(\mathbf{r}-\mathbf{r}',\omega) = \frac{e^{ik|\mathbf{r}-\mathbf{r}\,|}}{|\mathbf{r}-\mathbf{r}'|}, \qquad (3)$$

is the solution to $(\nabla^2+k^2)G(\mathbf{r}-\mathbf{r}',\omega) = -4\pi\delta^{(3)}(\mathbf{r}-\mathbf{r}')$. In the far-field approximation, $|\mathbf{r}-\mathbf{r}'| \approx r - \frac{\mathbf{k}_s}{k}\cdot\mathbf{r}'$, where $\mathbf{k}_s$ is a vector of magnitude k in the direction of the scattered field, and the Green's function simplifies to

$$G(\mathbf{r}-\mathbf{r}',\omega) \approx \frac{e^{ikr}}{r}e^{-i\mathbf{k}_s\cdot\mathbf{r}}\,. \qquad (4)$$

Noting that $U_s(\mathbf{r},\omega) = \frac{e^{ikr}}{r}f(\mathbf{k}_s,\mathbf{k}_i)$, where $f(\mathbf{k}_s,\mathbf{k}_i)$ is the scattering amplitude, for an incident plane wave of the form $U_i(\mathbf{r}',\omega) = e^{\mathbf{k}_i\cdot\mathbf{r}}$, Eq. (2) reduces to

$$f(\mathbf{k}_s,\mathbf{k}_i) = \int d^3r' F(\mathbf{r}',\omega)e^{-i(\mathbf{k}_s-\mathbf{k}_i)\cdot\mathbf{r}} + \int d^3r' F(\mathbf{r}',\omega)U_s(\mathbf{r}',\omega). \qquad (5)$$

Equation (5) is the LS equation. It is difficult to solve in general because the scattered field inside the scattering volume is unknown. In the first Born approximation, $U_s(\mathbf{r}', \omega)$ is set equal to zero, leading to a Fourier transform relationship between the scattering amplitude and the potential [24, 27]. For improved accuracy, the solution obtained with the first Born approximation (and subsequent solutions) can be used as the internal field, leading to the Liouville-Neumann series. However, this series only converges for small potentials, so it is not applicable to resonant structures, the focus of this work.

The EFA assumes the internal field is a spherical wave with the same scattering amplitude as the far-field scattering amplitude, i.e.,

$$U_s(\mathbf{r}', \omega) = \frac{e^{ikr}}{r'} f(\mathbf{k}_s, \mathbf{k}_i). \tag{6}$$

This allows the second term on the right hand side of Eq. (5) to be factorized, resulting in the following closed-form expression for the scattering amplitude:

$$f(\mathbf{k}_s, \mathbf{k}_i) = \frac{\int d^3r' F(\mathbf{r}', \omega) e^{-i(\mathbf{k}_s - \mathbf{k}_i)\cdot\mathbf{r}}}{1 - \int d^3r' F(\mathbf{r}', \omega) e^{-i\mathbf{k}_s\cdot\mathbf{r}} \frac{e^{ikr}}{r}}. \tag{7}$$

Equation (7) gives the scattering amplitude as a function of the potential. In principle, it is valid for arbitrary potentials. For small scattering potentials, the denominator is one and Eq. (7) reduces to the well-known expression obtained with the first-Born approximation. In forward scattering problems, $F(\mathbf{r}', \omega)$ is known and Eq. (7) can be used to calculate the scattering amplitude. Alternatively, in inverse scattering problems, $f(\mathbf{k}_s, \mathbf{k}_i)$ is known and $F(\mathbf{r}', \omega)$ can be determined. Defining the momentum transfer as $\mathbf{q} \equiv \mathbf{k}_s - \mathbf{k}_i$ and taking the Fourier transform of Eq. (7) with respect to $\mathbf{q}$, we obtain

$$F(\mathbf{r}, \omega) = F_B(\mathbf{r}, \omega) \left[1 - \int d^3r' F(\mathbf{r}', \omega) e^{-i\mathbf{k}_s\cdot\mathbf{r}} \frac{e^{ikr}}{r}\right] \tag{8}$$

where

$$F_B(\mathbf{r}, \omega) \equiv \frac{1}{(2\pi)^3} \int d^3q e^{i\mathbf{q}\cdot\mathbf{r}} f(\mathbf{k}_s, \mathbf{k}_i) \tag{9}$$

is the potential obtained using the first Born approximation. By iteratively substituting $F(\mathbf{r}, \omega)$ in Eq. (8) and applying the infinite geometric series sum, we obtain

$$F(\mathbf{r}, \omega) = \frac{F_B(\mathbf{r}, \omega)}{1 + \int d^3r' F_B(\mathbf{r}', \omega) e^{-i\mathbf{k}_s\cdot\mathbf{r}} \frac{e^{ikr}}{r}}. \tag{10}$$

The closed-form expressions in Eq. (7) and (10) form the basis for direct and inverse scattering studies, respectively. Their accuracy depends on the validity of the EFA and the requirement that the absolute value of the integral in the denominator of Eq. (10) is less than 1 for series convergence.

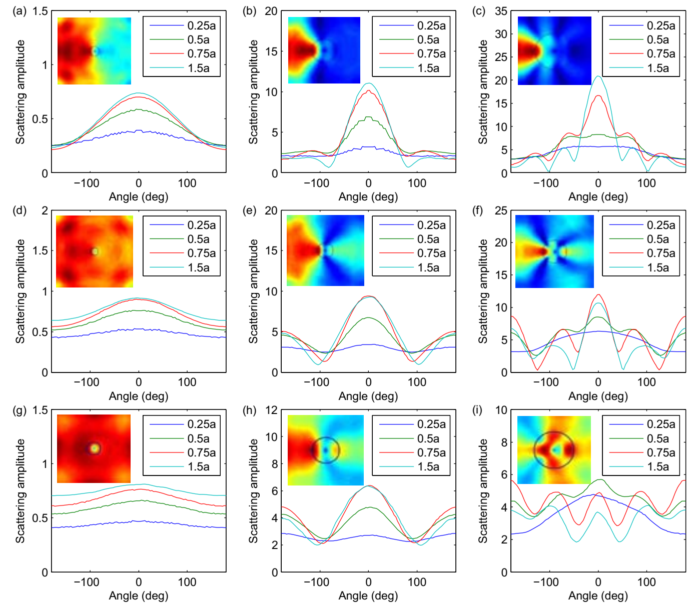

FIG. 1. Calculated scattering amplitude at different distances from the center of dielectric cylinders with $\epsilon = 2$ (top), $\epsilon = 6$ (middle), and $\epsilon = 10$ (bottom) and diameters of $2ak\sqrt{\epsilon}=1$ (left), 2 (middle), and 3 (right).

While the formalism developed thus far is valid for quantum mechanical, electromagnetic, and acoustic scattering problems, to demonstrate the validity of our approach, we consider electromagnetic scattering, in which case $F(\mathbf{r}, \omega) = k^2[\epsilon(\mathbf{r}, \omega) - 1]/4\pi$, where $\epsilon(\mathbf{r}, \omega)$ is the relative permittivity of the scatterer. Using full-wave simulations, we calculated the scattering amplitude for infinite cylinders of radius a and frequency-independent homogeneous permittivity ϵ_r. To compare these results to our scalar-wave formalism, we consider light polarized along the axis of the cylinder. The calculated scattering amplitude at different distances from the center of cylinders with $\epsilon_r = 2$ (top), $\epsilon_r = 6$ (middle), and $\epsilon_r = 10$ (bottom) and diameters of $2ak\sqrt{\epsilon_r}=1$ (left), 2 (middle), and 3 (right) are shown in Fig. 1. Consistent with the EFA, we find that the scattering amplitude inside the cylinders is very close to the far-field values essentially for all cases except very close to the origin ($r < 0.5a$). To confirm the validity of EFA is not limited to scatterers with circular symmetry, we carried out a similar study for infinite square rods of side length $2w$. The calculated scattering amplitude at different distances from the rods are shown in Fig. 2. We find that the EFA is equally valid for this case for distances of $r < 0.5w$.

Having confirmed the validity and limitations of the EFA, we used Eq. (7) to calculate the scattering amplitude and cross section of scalar waves for a sphere with $\epsilon_r = 10$ and compared the results to the exact solution obtained by partial wave analysis, i.e., decomposing the wave function into spherical harmonics and imposing

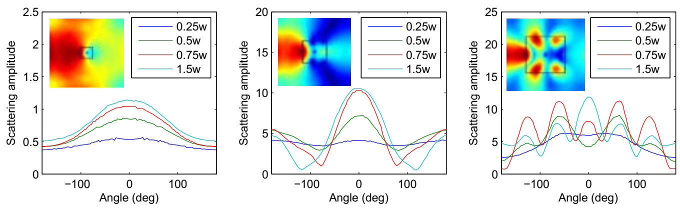

FIG. 2. Calculated scattering amplitude at different distances from the center of infinitely long square rods with $\epsilon = 6$ and side lengths of $2wk\sqrt{\epsilon} = 1$ (left), 2 (middle), and 3 (right).

continuity of the field and its derivative. The EFA leads to the following closed-form expression for the scattering amplitude:

$$f(q,k) = -\frac{(\epsilon_r - 1)k^2}{q^3} \frac{\sin qa - qa\cos qa}{1 + \frac{1}{4}(\epsilon_r - 1)(e^{i2ka} - i2ka - 1)} \tag{11}$$

Figure 3 shows the scattering cross section as a function of wavenumber (divided by the diameter $2a$) obtained by integrating Eq. (11) over angle as $2\pi \int_0^{2k} dq \frac{q}{k} |f(q,k)|^2$ (green). Also shown is the exact cross section calculated using partial wave analysis (blue). The values calculated using the first Born approximation are shown in red. For small wavenumbers, or long wavelengths, corresponding to Rayleigh scattering, all three calculations are in agreement. As the wavenumber increases, the Born method remains valid for $2ka/\pi < 0.4$, while the EFA remains valid for $2ka/\pi < 1.6$. In addition, the EFA accurately predicts both the location of the fundamental resonance around $2ka/\pi = 1$, corresponding to the isotropic monopole resonance, and its magnitude. On the other hand, the Born approximation fails near resonance, predicting an increasing cross section for all wavenumbers. The second resonance is not predicted with EFA, consistent with the results shown in Fig. 1. Also shown is the cross section obtained with EFA calculated using the optical theorem as $\frac{4\pi}{k} \Im f(0,k)$ (cyan). We find excellent agreement with the cross section obtained by angle integration, confirming that the EFA satisfies the optical theorem for this case. The accuracy of the EFA for homogeneous spheres can be understood from the field plots of Fig. 1. In regions where the EFA is invalid, near the center of the scatterer, the fields are close to zero, so their contribution to the scattered field, according to Eq. (2), is small. On the other hand, the results obtained with EFA may be less accurate for inhomogeneous potentials that increase near the origin.

The analytical expression in Eq. (10) can be used for inverse scattering studies. For validation we consider spheres, which allows us to use partial wave analysis to obtain the scattering amplitude for all values of q. This expression is then used in Eqs. (9) and (10) to obtain the permittivity reconstruction. The accuracy of this reconstruction is limited by the maximum spatial frequency of

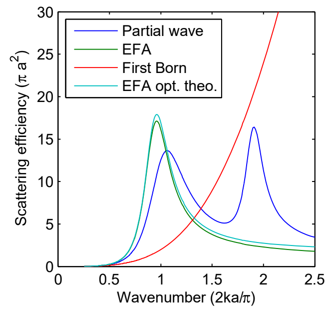

FIG. 3. Scattering cross section, in units of the cross sectional area, as a function of wavenumber for a sphere with $\epsilon = 10$, calculated using partial-wave analysis, EFA, and the first-Born approximation. The cross section obtained by applying the optical theorem to the EFA scattering amplitude is also shown.

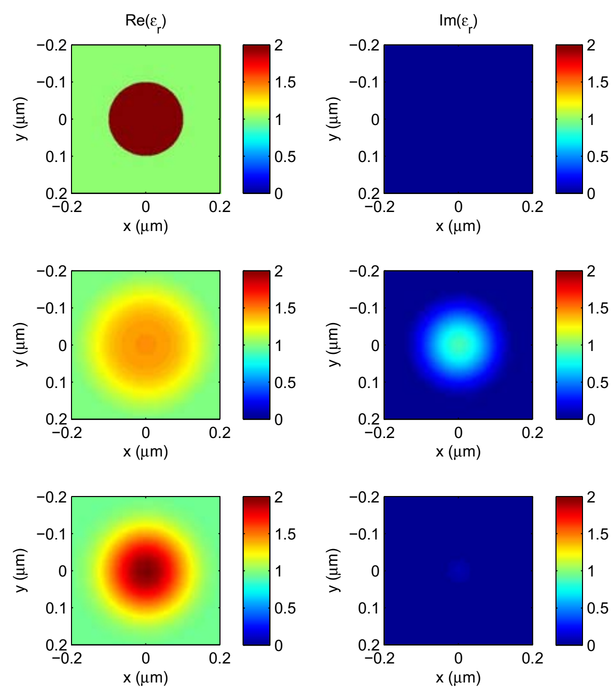

FIG. 4. Real (left panel) and imaginary (right panel) part of ϵ used in direct scattering (top panel) and reconstructions obtained by inverse scattering using first Born (middle panel) and EFA (bottom panel) methods for $\epsilon = 2$.

the scattered field, i.e., the limit of the integral in Eq. (9). Ideally, the shortest possible wavelength is used. However, for spheres the EFA appears to be valid only for $2ka/\pi < 1.6$ (Fig. 3). Therefore, the integral in Eq. (9) is performed for $q < 1.6\pi/a$. We also confirmed that the absolute value of the integral in the denominator of Eq. (10) is less than 1, a requirement for series convergence. Figures 4 through 6 compare the EFA-calculated real (left) and imaginary (right) parts of the permittivity distribution with the actual values and those obtained with the first Born approximation.

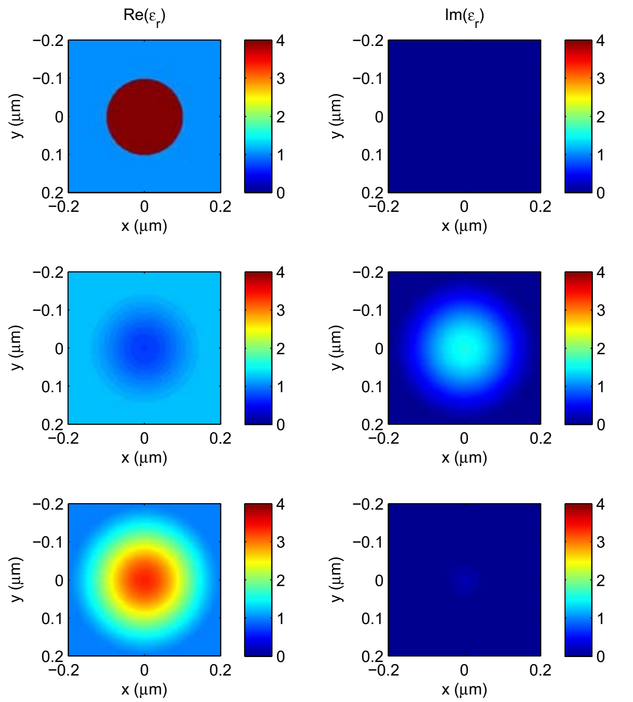

FIG. 5. Real (left panel) and imaginary (right panel) part of ϵ used in direct scattering (top panel) and reconstructions obtained by inverse scattering using first Born (middle panel) and EFA (bottom panel) methods for $\epsilon = 4$.

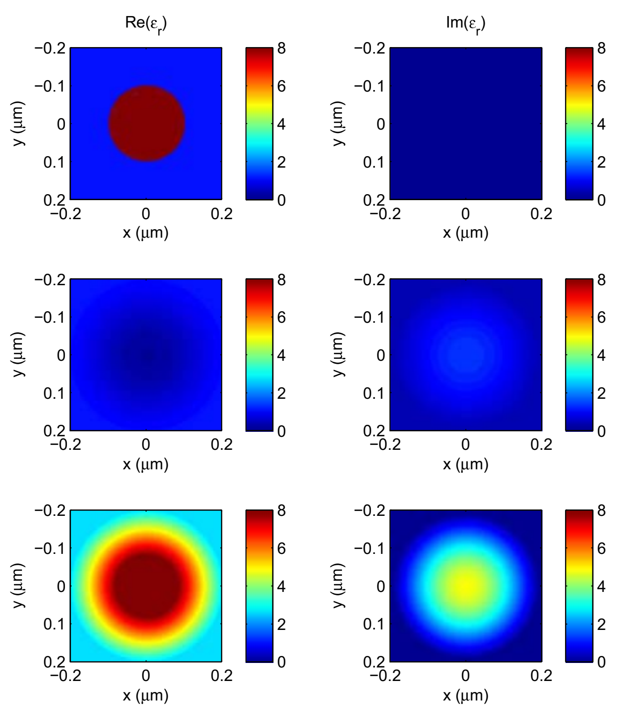

FIG. 6. Real (left panel) and imaginary (right panel) part of ϵ used in direct scattering (top panel) and reconstructions obtained by inverse scattering using first Born (middle panel) and EFA (bottom panel) methods for $\epsilon = 8$.

For $\epsilon_r = 2$ (Fig. 4), the scattering is weak and the real part predicted using the first Born approximation agrees reasonably well with the actual values. However, the imaginary part is non-zero near the center. The EFA is considerably more accurate with respect to both the real and imaginary parts of ϵ_r. The EFA reconstruction is slightly unresolved due to the limited spatial frequency used in the inversion.

For $\epsilon_r = 4$ (Fig. 5), the scattering is stronger and, expectedly, the prediction obtained with the Born approximation is poor, both the real and imaginary parts. The EFA continues to correctly predict purely real permittivity. The calculated values agree reasonably well with the actual values, though with less resolution compared to the previous case. Increasing the resolution would require a larger q limit, but this would cause the series to diverge, leading to worse agreement. Despite this limitation, the EFA is reasonably accurate for this case.

For $\epsilon = 8$ (Fig. 6), the scattering is even stronger and again the Born approximation fails to predict the correct permittivity. Although the EFA predicts the real part and shape reasonable well, it predicts unacceptably large imaginary part. This is because the scattering potential, proportional to $\epsilon_r - 1$, is large for this case, which limits the maximum value of q that can be used before the denominator term in Eq. (10) approaches 1, in which case the series sum diverges. Thus, for this strong scattering regime, inverse scattering with EFA only provides qualitative predictions.

In summary, we obtained a nonperturbative closed-form solution to the Lippmann-Schwinger scattering equation by assuming the scattered field within the scattering volume is a spherical wave with a scattering amplitude equal to the far-field scattering amplitude. We found this approximation to be largely valid for both spherical and non-spherical scatterers, and that the calculated scattering cross sections agree reasonably well with exact results for spheres, even through the fundamental resonance. The closed-form expression also enables reconstruction of the scatterer profile in inverse scattering studies. We applied this approach to reconstruct the permittivity profile of spheres and showed that the EFA approximation yields considerable improvement over the Born approximation. The simplicity, generality, and accuracy of our method suggest it can be a reliable and efficient tool for understanding a wide range of scattering problems in physics.

ACKNOWLEDGMENT

The authors are grateful to Dr. Michael Fiddy for several critical fruitful discussions on this topic and to DARPA for funding through Contract # HR001117C0118.

* Corresponding author: brian.slovick@sri.com

[1] R. G. Newton, *Scattering theory of waves and particles* (Springer Science and Business Media, 2013).
[2] J. Behura, K. Wapenaar, and R. Snieder, Geophys. **79**, A19 (2014).
[3] B. A. Slovick, Z. G. Yu, and S. Krishnamurthy, Phys. Rev. B **89**, 155118 (2014).
[4] G. Bao, P. Li, J. Lin, and F. Triki, Inverse Problems **31**, 31 (2015).
[5] H. W. Levinson and V. A. Markel, Phys. Rev. E **94**, 043318 (2016).
[6] M. J. Ablowitz and Z. Z. H. Musslimani, Nonlinearity **29**, 915 (2016).
[7] J. R. Taylor, *Scattering theory: the quantum theory of nonrelativistic collisions* (Courier Corporation, 2016).
[8] K. Chadan and P. C. Sabatier, *Inverse problems in quantum scattering theory* (Springer Science and Business Media, 2017).
[9] D. Colton, J. Coyle, and P. Monk, Siam Review **42**, 369 (2000).
[10] D. Colton and R. Kress, *Inverse acoustic and electromagnetic scattering theory* (Springer Science & Business Media, 2012).
[11] H. W. Levinson and V. A. Markel, Phys. Rev. E **94**, 043317 (2016).
[12] V. Isakov, *Scattering Problems and Stationary Waves. In Inverse Problems for Partial Differential Equations* (Springer, 2017).
[13] D. Colton, H. Haddar, and M. Piana, Inverse Probl. **19**, S105 (2003).
[14] G. Leone and F. Soldovieri, IEEE Trans. Geosci. Remote Sens. **41**, 66 (2003).
[15] I. H. Woodhouse, *Introduction to microwave remote sensing* (CRC Press, 2017).
[16] T. S. Ralston, D. L. Marks, P. S. Carney, and S. A. Boppart, JOSA A **23**, 1027 (2006).
[17] D. L. Marks, T. S. Ralston, S. A. Boppart, and P. S. Carney, JOSA A **24**, 1034 (2007).
[18] M. A. Fiddy and M. Testorf, Opt. Exp. **14**, 2037 (2006).
[19] R. C. Rumpf, M. A. Fiddy, and M. E. Testorf, Opt. Exp. **15**, 4735 (2007).
[20] N. G. Alexopoulos, C. A. Kyriazidou, and H. F. Contopanagos, IEEE Trans. Microw. Theory Tech. **55**, 254 (2007).
[21] L. D. Donato, T. Isernia, G. Labate, and L. Matekovits, Sci. Rep. **7**, 3680 (2017).
[22] J. Cheng, S. Inampudi, and H. Mosallaei, Sci. Rep. **7**, 12228 (2017).
[23] R. H. Landau, *Quantum Mechanics II: A Second Course in Quantum Theory 2nd Edition* (Wiley, 1996).
[24] A. J. Devaney, Opt. Lett. **7**, 111 (1982).
[25] A. J. Devaney and M. L. Oristaglio, Phys. Rev. Lett. **51**, 237 (1983).
[26] G. Vainikko, *Fast solvers of the Lippmann-Schwinger equation. In Direct and inverse problems of mathematical physics* (Springer, 2000).
[27] M. Born and E. Wolf, *Principles of Optics* (Cambridge, 1999).
[28] M. A. Fiddy and R. S. Ritter, *Introduction to Imaging from Scattered Fields* (CRC Press, 2015).

APPENDIX D:
INVERSE SCATTERING FROM TIME-VARIANT MEDIA

Frequency conversion conditions:
We start from Maxwell's equations in the absence of free charges:

$$
\begin{aligned}
&\nabla \times \mathbf{E}(\mathbf{r},t) = -\frac{\partial \mathbf{B}(\mathbf{r},t)}{\partial t} \\
\Rightarrow \quad &\nabla \times (\nabla \times \mathbf{E}(\mathbf{r},t)) = -\frac{\partial (\nabla \times \mathbf{B}(\mathbf{r},t))}{\partial t} \\
\Rightarrow \; &\nabla[\nabla \cdot \mathbf{E}(\mathbf{r},t)] - \nabla^2 \mathbf{E}(\mathbf{r},t) = -\mu_0 \frac{\partial^2 \mathbf{D}(\mathbf{r},t)}{\partial t^2} \\
\Rightarrow \quad &\nabla^2 \mathbf{E}(\mathbf{r},t) = \mu_0 \frac{\partial^2 \mathbf{D}(\mathbf{r},t)}{\partial t^2}
\end{aligned}
\tag{D1}
$$

The displacement field **D** is related to the linear susceptibility χ and polarization **P** by:

$$
\begin{aligned}
\mathbf{D}(\mathbf{r},t) &= \varepsilon_0 (1+\chi)\mathbf{E}(\mathbf{r},t) \\
&= \varepsilon_0 \mathbf{E}(\mathbf{r},t) + \mathbf{P}(\mathbf{r},t)
\end{aligned}
\tag{D2}
$$

Substituting Eq. D2 in Eq. D1 and using $\mu_0\varepsilon_0 = c^2$, we get the well-known form of the time-dependent wave equation for the electric field in an inhomogeneous and isotropic medium:

$$\left(\nabla^2 - \frac{1}{c^2}\frac{\partial^2}{\partial t^2}\right)\mathbf{E}(\mathbf{r},t) = \mu_0 \frac{\partial^2 \mathbf{P}(\mathbf{r},t)}{\partial t^2} \tag{D3}$$

The polarization $\mathbf{P}(\mathbf{r},t)$ of the medium is the source of scattering. In a linear medium, the relationship between the polarization and the electric field is:

$$\mathbf{P}(\mathbf{r},t) = \varepsilon_0 \int_{-\infty}^{\infty} dt' \, \chi(t,t')\mathbf{E}(\mathbf{r},t'), \tag{D4}$$

where χ is the linear susceptibility of the medium, whose Fourier transform is given by:

$$\chi(\omega) = \int_{-\infty}^{\infty} dt \;\; \chi(t) e^{i\omega t} \,. \tag{D5}$$

Equation Eq. D4 states the polarization at time t depends on the electric field at all past times, which is a consequence of the fact that the medium does not respond instantaneously to the field.

Case 1: Time-<u>invariant</u> medium with frequency independent χ and ε

In this case, the medium is time invariant, and χ has a constant value such that:

$$\chi(t,t') = \chi(t-t') = \chi_0 \delta(t-t') \,. \tag{D6}$$

Then from Eq. D5, $\chi(\omega) = \chi_0$. The polarization from Eq. (4) is:

$$\mathbf{P}(\mathbf{r},t) = \varepsilon_0 \int_{-\infty}^{\infty} dt' \chi_0 \delta(t-t')\mathbf{E}(\mathbf{r},t') = \varepsilon_0 \chi_0 \mathbf{E}(\mathbf{r},t) \,. \tag{D7}$$

Substituting Eq. D7 in Eq. D3, we get the wave equation for a time invariant, isotropic, homogeneous medium with no dispersion:

$$\left(\nabla^2 - \frac{\varepsilon}{c^2}\frac{\partial^2}{\partial t^2}\right)\mathbf{E}(\mathbf{r},t) = 0 \tag{D8}$$

Case 2: Time-<u>invariant</u> medium with frequency dependent χ and ε (temporal dispersion)

Since the medium is time invariant,

$$\chi(t,t') = \chi(t-t') \tag{D9}$$

We further express $\mathbf{E}(\mathbf{r},t)$ in terms of its Fourier transform as:

$$\mathbf{E}(\mathbf{r},t) = \int_{-\infty}^{\infty} d\omega\, \mathbf{E}(\mathbf{r},\omega)\, e^{-i\omega t} \tag{D10}$$

Then polarization from Eq. D4 is:

$$\begin{aligned}
\mathbf{P}(\mathbf{r},t) &= \varepsilon_0 \int_{-\infty}^{\infty} d\omega\, \mathbf{E}(\mathbf{r},\omega) \int_{-\infty}^{\infty} dt'\, \chi(t-t') e^{-i\omega t'} \\
&= \varepsilon_0 \int_{-\infty}^{\infty} d\omega\, \mathbf{E}(\mathbf{r},\omega) e^{-i\omega t} \int_{-\infty}^{\infty} d\tau\, \chi(\tau)\, e^{i\omega\tau} \\
&= \varepsilon_0 \int_{-\infty}^{\infty} d\omega\, \mathbf{E}(\mathbf{r},\omega)\, \chi(\omega)\, e^{-i\omega t}
\end{aligned} \tag{D11}$$

Substituting Eq. (D11) and (D10) in Eq. (D3) we obtain:

$$\int_{-\infty}^{\infty} d\omega e^{-i\omega t}\left[\left(\nabla^2 + k^2\right)\mathbf{E}(\mathbf{r},\omega) + k^2\chi(\omega)\mathbf{E}(\mathbf{r},\omega)\right] = 0 \tag{D12}$$

where $k=\omega/c$. Since the Fourier transform of an integrable function $f(\omega)$ is zero if and only if $f(\omega)=0$, the integrand in Eq. D12 must be zero for each frequency component and we obtain:

$$\begin{aligned}
\left(\nabla^2 + k^2\right)\mathbf{E}(\mathbf{r},\omega) &= -4\pi k^2 \frac{\chi(\omega)}{4\pi}\mathbf{E}(\mathbf{r},\omega) \\
&= -4\pi k^2 \frac{\left[\varepsilon(\omega) - 1\right]}{4\pi}\mathbf{E}(\mathbf{r},\omega)
\end{aligned} \tag{D13}$$

Equation (D13) is the well-known inhomogeneous Helmholtz equation for dispersive media. It forms the basis of inverse scattering theory for time-invariant media. Importantly, because Eq. (D13) must be satisfied for each frequency component $\mathbf{E}(\mathbf{r},\omega)$ independently, there is no coupling between different frequency components. Therefore, a time-invariant medium cannot scatter light to frequencies different from the incident frequency.

Case 3: Time-<u>variant</u> medium

This case corresponds to materials whose dielectric function is temporally modulated externally or by internal processes independent on the incident field. In this case, the value of χ at a time t is instantaneous and does not depend on the value of the electric field at previous times t'. This can be expressed as:

$$\chi(t,t') = \chi(t')\delta(t-t'). \tag{D14}$$

As a result, the polarization from Eq. D4 is given by the product of χ and $\mathbf{E}$ at time t:

$$\mathbf{P}(\mathbf{r},t) = \varepsilon_0 \int_{-\infty}^{\infty} dt' \chi(t')\delta(t-t')\mathbf{E}(\mathbf{r},t') = \varepsilon_0 \chi(t)\mathbf{E}(\mathbf{r},t)\,. \tag{D15}$$

Then the wave equation (Eq. 3) can be written as:

$$\left(\nabla^2 - \frac{1}{c^2}\frac{\partial^2}{\partial t^2}\right)\mathbf{E}(\mathbf{r},t) = \frac{1}{c^2}\frac{\partial^2}{\partial t^2}\left[\chi(t)\mathbf{E}(\mathbf{r},t)\right]. \tag{D16}$$

As before (Eq. D10), substituting the Fourier transform of $\mathbf{E}(\mathbf{r},t)$, the LHS of Eq. D16 becomes:

$$\left(\nabla^2 - \frac{1}{c^2}\frac{\partial^2}{\partial t^2}\right)\mathbf{E}(\mathbf{r},t) = \int_{-\infty}^{\infty} d\omega \left(\nabla^2 + k^2\right)\mathbf{E}(\mathbf{r},\omega)\, e^{-i\omega t} \tag{D17}$$

Similarly, substituting the Fourier transform of $\mathbf{E}(\mathbf{r},t)$ in Eq. 16 along with the FT of χ,

$$\chi(t) = \int_{-\infty}^{\infty} d\omega\ \chi(\omega)\, e^{-i\omega t} \tag{D18}$$

We get,

$$\begin{aligned}
\frac{1}{c^2}\frac{\partial^2}{\partial t^2}\left[\chi(t)\mathbf{E}(\mathbf{r},t)\right] &= \frac{1}{c^2}\frac{\partial^2}{\partial t^2}\left[\int_{-\infty}^{\infty} d\omega' \chi(\omega')\, e^{-i\omega' t} \int_{-\infty}^{\infty} d\Omega \mathbf{E}(\mathbf{r},\Omega)\, e^{-i\Omega t}\right] \\
&= \frac{1}{c^2}\frac{\partial^2}{\partial t^2}\int_{-\infty}^{\infty} d\omega' \chi(\omega') \int_{-\infty}^{\infty} d\Omega \mathbf{E}(\mathbf{r},\Omega) e^{-i(\omega'+\Omega)t} \\
&= \frac{1}{c^2}\frac{\partial^2}{\partial t^2}\int_{-\infty}^{\infty} d\omega' \chi(\omega') \int_{-\infty}^{\infty} d\omega \mathbf{E}(\mathbf{r},\omega-\omega') e^{-i\omega t} \\
&= -\int_{-\infty}^{\infty} d\omega e^{-i\omega t}\, \frac{\omega^2}{c^2} \int_{-\infty}^{\infty} d\omega' \chi(\omega')\mathbf{E}(\mathbf{r},\omega-\omega')
\end{aligned} \tag{D19}$$

Substituting Eq. D17 and D19 into Eq. D16 leads to:

$$\int_{-\infty}^{\infty} d\omega e^{-i\omega t}\left[\left(\nabla^2 + k^2\right)\mathbf{E}(\mathbf{r},\omega) + k^2 \int_{-\infty}^{\infty} d\omega'\ \chi(\omega')\mathbf{E}(\mathbf{r},\omega-\omega')\right] = 0 \tag{D19}$$

As before, the FT in Eq. D19 is zero if and only if the integrand is zero, leaving:

$$\left(\nabla^2 + k^2\right)\mathbf{E}(\mathbf{r},\omega) = -k^2 \int_{-\infty}^{\infty} d\omega'\, \chi(\omega')\mathbf{E}(\mathbf{r},\omega-\omega') \tag{D20}$$

The total field **E** is the sum of incident field $\mathbf{E_i}$ and scattered field $\mathbf{E_s}$**.** Since $\mathbf{E_i}$ is the solution of LHS, we re-write Eq. D20 as:

$$\left(\nabla^2 + k^2\right)\mathbf{E}_S(\mathbf{r},\omega) = -4\pi\, \frac{k^2}{4\pi} \int_{-\infty}^{\infty} d\omega'\, \chi(\omega')\mathbf{E}(\mathbf{r},\omega-\omega') \tag{D21}$$

We find that, in contrast to time-invariant media, the source term is given by the convolution of χ with **E**. As a result, the field at ω depends on the field at all other frequencies ω-ω', allowing for the possibility of frequency conversion in linear materials. The Eq. D21 will be solved for more general solution using Green's function (GF) approach, which is developed in next section.

$$\mathbf{E}_S(\mathbf{r},\omega) = \frac{k^2}{4\pi}\int d^3r' \int dt' G(r,r') \int_{-\infty}^{\infty} d\omega' \chi(r',\omega')\mathbf{E}(\mathbf{r}',\omega-\omega') \tag{D22}$$

With the GF defined previously, and employing far field approximation, Eq. D22 becomes:

$$\begin{aligned}\mathbf{E}_S(\mathbf{r},\omega) &= \frac{k^2}{4\pi}\int d^3r' \frac{e^{ik|\mathbf{r}-\mathbf{r}'|}}{|\mathbf{r}-\mathbf{r}'|}\int_{-\infty}^{\infty} d\omega' \chi(r',\omega')\mathbf{E}(\mathbf{r}',\omega-\omega') \\ &\approx \frac{k^2}{4\pi}\frac{e^{ikr}}{r}\int d^3r' e^{ik_s\cdot r'}\int_{-\infty}^{\infty} d\omega' \chi(r',\omega')\mathbf{E}(\mathbf{r}',\omega-\omega')\end{aligned} \tag{D23}$$

The total field is the sum of incident field at ω_i and scattered field. Thus,

$$\mathbf{E}(\mathbf{r},\omega'') = E_i(r,\omega'')\delta(\omega''-\omega_i) + E_S(r,\omega'') \tag{D24}$$

Substituting Eq. D24 in Eq. D23, we get:

$$\begin{aligned}\mathbf{E}_S(\mathbf{r},\omega) &= \frac{k^2}{4\pi}\frac{e^{ikr}}{r}\int d^3r' e^{-ik_s\cdot r'}\int_{-\infty}^{\infty} d\omega' \chi(r',\omega')\mathbf{E}_i(\mathbf{r}',\omega-\omega')\delta(\omega-\omega'-\omega_i) \\ &\quad+\frac{k^2}{4\pi}\frac{e^{ikr}}{r}\int d^3r' e^{-ik_s\cdot r'}\int_{-\infty}^{\infty} d\omega' \chi(r',\omega')\mathbf{E}_S(\mathbf{r}',\omega-\omega') \\ &= \frac{k^2}{4\pi}\frac{e^{ikr}}{r}\int d^3r' e^{-ik_s\cdot r'} \chi(r',\omega-\omega_i)e^{ik_i\cdot r'} \\ &\quad+\frac{k^2}{4\pi}\frac{e^{ikr}}{r}\int d^3r' e^{-ik_s\cdot r'}\int_{-\infty}^{\infty} d\omega' \chi(r',\omega')\mathbf{E}_S(\mathbf{r}',\omega-\omega')\end{aligned} \tag{D25}$$

Applying the extended far-field approximation,

$$\mathbf{E}_S(\theta',\varphi',\omega) = \mathbf{E}_S(\theta,\varphi,\omega) \tag{D26}$$

and assuming the angular distribution at ω and ω-ω' are similar (because of small frequency shift)—and collecting like terms, we get:

$$\begin{aligned}\mathbf{E}_S(\mathbf{r},\omega) &= \frac{k^2}{4\pi}\frac{e^{ikr}}{r}\int d^3r' e^{-iq\cdot r'} \chi(r',\omega-\omega_i) \\ &\quad+\frac{k^2}{4\pi}\mathbf{E}_S(\mathbf{r},\omega)\int d^3r' e^{-ik_s\cdot r'}\frac{e^{ikr'}}{r'}\int_{-\infty}^{\infty} d\omega' \chi(r',\omega') \\ \Rightarrow \mathbf{E}_S(\mathbf{r},\omega) &= \frac{\frac{k^2}{4\pi}\frac{e^{ikr}}{r}\int d^3r' e^{-iq\cdot r'} \chi(r',\omega-\omega_i)}{1-\frac{k^2}{4\pi}\int d^3r' e^{-ik_s\cdot r'}\frac{e^{ikr'}}{r'}\int_{-\infty}^{\infty} d\omega' \chi(r',\omega')}\end{aligned} \tag{D27}$$

We can evaluate Eq. D27 for various output frequencies. First, we evaluate for $\omega=\omega_i$. The χ in the numerator is now evaluated at zero frequency, which is the unperturbed part of the susceptibility given by χ_0. The ω' integral of the cyclic function in the denominator is zero, leaving only the DC component which is also χ_0. Hence Eq. 46 is simply,

$$\mathbf{E}_S(\mathbf{r},\omega_i) = \frac{\frac{k_i^2}{4\pi}\frac{e^{ik_i r}}{r}\int d^3r' e^{-iq\cdot r'}\chi_0(r')}{1-\frac{k_i^2}{4\pi}\int d^3r' e^{-ik_s\cdot r'}\frac{e^{ikr'}}{r'}\chi_0(r')} \tag{D28}$$

Next we evaluate at displaced frequency $\omega=\omega_i\pm\Omega$, when χ has specific time dependence— $\chi_0+\Delta\left(e^{i\Omega t}+e^{-i\Omega t}\right)$. The χ in the numerator of Eq. D27 is at the frequency $\pm\Omega$, and hence has a value of Δ (perturbation to susceptibility). As before, the ω' integral in the denominator results in χ_0 and hence,

$$\mathbf{E}_S(\mathbf{r},\omega_i\pm\Omega) = \frac{\frac{k_\pm^{\ 2}}{4\pi}\frac{e^{ik_\pm r}}{r}\int d^3r' e^{-iq_\pm\cdot r'}\Delta(r')}{1-\frac{k_\pm^{\ 2}}{4\pi}\int d^3r' e^{-ik_s\cdot r'}\frac{e^{ik_\pm r'}}{r'}\chi_0(r')} \tag{D29}$$

The Eqs. D27-D29 can be inverted to obtain $\chi(r,\omega)$ in terms of $E_s(r,\omega)$ following the steps described in Eq. B6 to Eq. B1) of Appendix B.

Example:

We can now consider a special case of temporal modulation of the form more explicitly:

$$\begin{aligned}\chi(t) &= \chi_0 + 2\Delta\cos(\Omega t)\\ &= \chi_0+\Delta\left(e^{i\Omega t}+e^{-i\Omega t}\right)\end{aligned} \tag{D30}$$

The FT of the modulation is given by:

$$\chi(\omega') = \int_{-\infty}^{\infty} dt e^{i\omega' t}\Delta\left(e^{i\Omega t}+e^{i\Omega t}\right) = \chi_0\delta(\omega')+\Delta\left[\delta(\omega'+\Omega)+\delta(\omega'-\Omega)\right]. \tag{D32}$$

The wave equation Eq. D21 becomes:

$$\left(\nabla^2+k^2\right)\mathbf{E}_S(\mathbf{r},\omega) = -k^2\chi_0\mathbf{E}(\mathbf{r},\omega)-k^2\Delta\left[\mathbf{E}(\mathbf{r},\omega+\Omega)+\mathbf{E}(\mathbf{r},\omega-\Omega)\right]. \tag{D33}$$

We find that, as a consequence of the modulation, the field at ω depends on that at $\omega\pm\Omega$. Consider the E field,

$$\mathbf{E}(\mathbf{r},\omega) = E_i(r,\omega)\delta(\omega-\omega_i)+E_S(r,\omega) \tag{D34}$$

substituting Eq. D34 into Eq. D33 for $\omega=\omega_i$ we get,

$$\left(\nabla^2+k^2\right)\mathbf{E}_S(\mathbf{r},\omega_i) = -k^2\chi_0\mathbf{E}(\mathbf{r},\omega_i)-k^2\Delta\left[\mathbf{E}_S(\mathbf{r},\omega_i+\Omega)+\mathbf{E}_S(\mathbf{r},\omega_i-\Omega)\right] \tag{D35}$$

Note there is no incident field at displaced frequencies, and further the equation reduces to the elastic case when Δ is zero. Similarly, the wave equations for the fields at $\omega+\Omega$ and $\omega-\Omega$ are:

$$\left(\nabla^2 + k_+^2\right)\mathbf{E}_S(\mathbf{r},\omega_i+\Omega) = -k_+^2\chi_0\mathbf{E}_S(\mathbf{r},\omega_i+\Omega) - k_+^2\Delta\,\mathbf{E}_i(\mathbf{r},\omega_i) - k_+^2\Delta\left[\mathbf{E}_S(\mathbf{r},\omega_i+2\Omega)+\mathbf{E}_S(\mathbf{r},\omega_i)\right] \quad , \tag{D46}$$

$$\left(\nabla^2 + k_-^2\right)\mathbf{E}_S(\mathbf{r},\omega_i-\Omega) = -k_-^2\chi_0\mathbf{E}_S(\mathbf{r},\omega_i-\Omega) - k_-^2\Delta\,\mathbf{E}_i(\mathbf{r},\omega_i) - k_-^2\Delta\left[\mathbf{E}_S(\mathbf{r},\omega_i-2\Omega)+\mathbf{E}_S(\mathbf{r},\omega_i)\right] \quad , \tag{D36}$$

where $k_\pm=(\omega\pm\Omega)/c$. It follows there will be an infinite number of coupled equations for the higher-order harmonics. If we consider only the first-order harmonics and ignore all second-order terms, we obtain three coupled equations,

$$\left(\nabla^2 + k^2\right)\mathbf{E}_S(\mathbf{r},\omega_i) = -k^2\chi_0\mathbf{E}_i(\mathbf{r},\omega_i) - k^2\chi_0\mathbf{E}_S(\mathbf{r},\omega_i), \tag{D38}$$

$$\left(\nabla^2 + k_+^2\right)\mathbf{E}_S(\mathbf{r},\omega_i+\Omega) = -k_+^2\chi_0\mathbf{E}_S(\mathbf{r},\omega_i+\Omega) - k_+^2\Delta\,\mathbf{E}_i(\mathbf{r},\omega_i), \tag{D39}$$

$$\left(\nabla^2 + k_-^2\right)\mathbf{E}_S(\mathbf{r},\omega_i-\Omega) = -k_-^2\chi_0\mathbf{E}_S(\mathbf{r},\omega_i-\Omega) - k_-^2\Delta\,\mathbf{E}_i(\mathbf{r},\omega_i). \tag{D40}$$

Note that Eq. D38 is identical to the elastic scattering case. Once $E_S(r, \omega_i)$ is determined from Eq. D38, it can be substituted in Eqs. D39 and D40 to solve for E_S at the displaced frequencies. Similar to the current inverse-scattering formalism, each of these equations can be recast as integral equations using Green's function. The main difference is that we must solve three loosely coupled integral equations.

Applying GF approach and extended far-field approximation (EFA) to Eq. D38,

$$\begin{aligned}\mathbf{E}_S(\mathbf{r},\omega) &= \frac{k^2}{4\pi}\frac{e^{ikr}}{r}\int d^3r'\, e^{-ik_s r'}\chi_0(r')\mathbf{E}_i(\mathbf{r}',\omega_i) + \frac{k^2}{4\pi}\frac{e^{ikr}}{r}\int d^3r'\, e^{-ik_s r'}\chi_0(r')\mathbf{E}_S(\mathbf{r}',\omega_i)\\ &= \frac{k^2}{4\pi}\frac{e^{ikr}}{r}\int d^3r'\, e^{-ik_s r'}\chi_0(r')\mathbf{E}_i(\mathbf{r}',\omega_i) + \frac{k^2}{4\pi}\mathbf{E}_S(\mathbf{r},\omega_i)\int d^3r'\, e^{-ik_s r'}\chi_0(r')\frac{e^{ikr'}}{r'}\end{aligned} \tag{D41}$$

$$\mathbf{E}_S(\mathbf{r},\omega_i) = \frac{\dfrac{k_i^2}{4\pi}\dfrac{e^{ik_i r}}{r}\displaystyle\int d^3r'\, e^{-iq\cdot r'}\chi_0(r')}{1+\dfrac{k_i^2}{4\pi}\displaystyle\int d^3r'\, e^{-ik_s\cdot r'}\dfrac{e^{ikr'}}{r'}\chi_0(r')} \tag{D42}$$

As we can see, Eq. D42 is identical to Eq. D28 obtained earlier. Similarly applying GF approach and EFA at the *same* frequencies to Eq. D39 and Eq. D40, leads to,

$$\mathbf{E}_S(\mathbf{r},\omega_i\pm\Omega) = \frac{\dfrac{k_\pm{}^2}{4\pi}\dfrac{e^{ik_\pm r}}{r}\displaystyle\int d^3r'\, e^{-iq_\pm\cdot r'}\Delta(r')}{1-\dfrac{k_\pm{}^2}{4\pi}\displaystyle\int d^3r'\, e^{-ik_s\cdot r'}\dfrac{e^{ik_\pm r'}}{r'}\chi_0(r')} \tag{D43}$$

It should be noted the scattering field in the left-hand side (LHS) and right-hand side (RHS) of Eq. D39 are at the same frequencies and the EFA is required to be applied at that frequency. Although this observation appears to be in conflict with the condition applied to arrive at Eq. D27) - Eq. D29 (requiring EFA application at displaced frequencies), the discard of $\omega\pm2\Omega$

terms essentially leads to the assumption the frequency displacement is small. The closed-form expression with EFA is justified only when the modulating frequency is much smaller than the incident frequency. This is normally the case for most of the problems.

Time-dependent Green's function approach for inverse scattering:
Next we solve the same problem as above, but with a time-dependent GF approach to get final expressions for field in terms of time, instead of frequency as derived earlier.
We shall now use the GF approach to solve the t-dependent wave equation [Eq. D16].

$$\left(\nabla^2 - \frac{1}{c^2}\frac{\partial^2}{\partial t^2}\right) G(\mathbf{r},t,r',t') = -4\pi\,\delta(r-r')\delta(t-t') \tag{D44}$$

Defining R=|**r**-**r'**| and τ=|t-t'|, we have

$$\begin{aligned} G(R,\tau) &= \int_{-\infty}^{\infty} G(R,\omega)\, e^{-i\omega t}\, d\omega \\ \delta(t) &= \int_{-\infty}^{\infty} e^{-i\omega t}\, d\omega \end{aligned} \tag{D45}$$

Substituting Eq. D44 in Eq. D45, we get

$$\begin{aligned} &\int \left(\nabla^2 + k^2\right) G(R,\omega)\, e^{-i\omega t}\, d\omega = -4\pi \int \delta(R)\, e^{-i\omega t}\, d\omega \\ &\Rightarrow \left(\nabla^2 + k^2\right) G(R,\omega) = -4\pi\,\delta(R) \\ &\Rightarrow G(R,\omega) = \frac{e^{ikR}}{R} = \frac{e^{ik|r-r'|}}{|r-r'|} \end{aligned} \tag{D46}$$

Hence the final solution is:

$$\mathbf{E}(\mathbf{r},t) = \frac{1}{c^2}\int d^3r' \int dt'\, G(r-r',t-t')\, \frac{\partial^2}{\partial t'^2}\left[\chi(\mathbf{r}',t')\mathbf{E}(\mathbf{r}',t')\right] \tag{D47}$$

Note that Eq. D47 is exact. However note that the integration over $\mathbf{r}'$ is non zero only where χ is non zero and is often restricted to meta-element volume. Although we can specify E(**r**,t) at far field for inverse scattering studies, the value of the field inside the meta-element is unknown. Hence this equation can be solved only under specific approximations.
The GF in time-domain is

$$\begin{aligned} G(r-r',\tau) &= \int_{-\infty}^{\infty} \frac{e^{ik|r-r'|}}{|r-r'|}\, e^{-i\omega\tau}\, d\omega \\ &= \frac{1}{|r-r'|}\int_{-\infty}^{\infty} e^{ik|r-r'|}\, e^{-i\omega\tau}\, d\omega \\ &= \frac{1}{|r-r'|}\,\delta\!\left(\tau - \frac{|r-r'|}{c}\right) \end{aligned} \tag{D48}$$

We consider three approximations. <u>First</u>, we assume χ(t) is slower varying function of t when compared to E(t). This is justified in cases where the shift in frequency is much smaller than the incident frequency.

$$\frac{\partial^2}{\partial t'^2}\left[\chi(t')\mathbf{E}(\mathbf{r}',t')\right]\approx \chi(t')\frac{\partial^2}{\partial t'^2}\left[\mathbf{E}(\mathbf{r}')e^{-i\omega t}\right]$$
$$= -\omega^2\chi(\mathbf{r}',t')\mathbf{E}(\mathbf{r}')e^{-i\omega t} \tag{D49}$$

Substituting Eq. D49 and D48 in Eq. D47, we get

$$\mathbf{E}(\mathbf{r},t) = -\frac{\omega^2}{c^2}\int d^3r' \int dt'\, \chi(r',t')\mathbf{E}(\mathbf{r}')e^{-i\omega t'}\frac{1}{|\mathbf{r}-\mathbf{r}'|}\delta\left(t-t'-\frac{|\mathbf{r}-\mathbf{r}'|}{c}\right)$$
$$= -k^2\int d^3r'\, \chi\left(r',t-\frac{r}{c}\right)\mathbf{E}(\mathbf{r}')e^{-i\omega t}\frac{e^{i(\omega/c)|\mathbf{r}-\mathbf{r}'|}}{|\mathbf{r}-\mathbf{r}'|} \tag{D50}$$
$$= -k^2\int d^3r'\, \chi\left(r',t-\frac{r}{c}\right)\mathbf{E}(\mathbf{r}',t)\frac{e^{ik|\mathbf{r}-\mathbf{r}'|}}{|\mathbf{r}-\mathbf{r}'|}$$

<u>Second</u>, we consider r >> r'. This is well justified as the observation location far away from the scattering medium. Under these approximations, we write

$$|\mathbf{r}-\mathbf{r}'| = \left[r^2 + r'^2 - 2\,\mathbf{r}\cdot\mathbf{r}'\right]^{1/2}$$
$$\approx r - \frac{\mathbf{r}}{r}\cdot\mathbf{r}' \tag{D51}$$
$$= r - \frac{\boldsymbol{k}}{k}\cdot\mathbf{r}'$$

Employing this approximation and noting that the field inside the integral is a sum of incident and the scattered field, the Eq. D50 reduces to

$$\mathbf{E}_S(\mathbf{r},t) = \frac{k^2}{4\pi}\frac{e^{ikr}}{r}\int d^3r'\, e^{-ik\cdot r'}\chi\left(r',t-\frac{r}{c}\right)\left[\mathbf{E}_i(\mathbf{r}',t)+\mathbf{E}_S(\mathbf{r}',t)\right] \tag{D52}$$

If we retain only the first term in the integral, that constitutes as a <u>third</u> approximation—commonly known as first Born approximation [$E_i(r') = e^{ik_i r'}e^{i\omega_i t}$]—and we get

$$\mathbf{E}(\mathbf{r},t) = \frac{k^2}{4\pi}\frac{e^{ikr}}{r}e^{i\omega_i t}\int d^3r'\, \chi\left(\mathbf{r}',t-\frac{r}{c}\right)e^{-i(\boldsymbol{k}-\boldsymbol{k}_i)\cdot r'}$$
$$\equiv \frac{k^2}{4\pi}\frac{e^{ikr}}{r}e^{i\omega_i t}\int d^3r'\, \chi\left(\mathbf{r}',t-\frac{r}{c}\right)e^{-i\mathbf{q}\cdot\mathbf{r}'} \tag{D53}$$

Then, χ can be determined by multiplying both sides with $e^{i\mathbf{q}\cdot\mathbf{r}}$ and integrating over **q.**

$$\int\frac{4\pi}{k^2}re^{-ikr}\mathbf{E}(\mathbf{r},t)\, e^{-i\omega_i t}\, e^{i\mathbf{q}\cdot\mathbf{r}}d^3q = -\int d^3r'\, \chi\left(\mathbf{r}',t-\frac{r}{c}\right)\int e^{-i\mathbf{q}\cdot(\mathbf{r}'-r)}\, d^3q$$
$$= -\chi\left(\mathbf{r},t-\frac{r}{c}\right)$$
$$\Rightarrow \chi(\mathbf{r},t) = \int\frac{4\pi}{k^2}re^{-ikr}\mathbf{E}(\mathbf{r},t)\, e^{-i\omega_i t}\, e^{i\mathbf{q}\cdot\mathbf{r}}d^3q\, e^{i\omega_i r/c} \tag{D54}$$
$$= \int\frac{4\pi}{k^2}re^{-i(k-k_i)r}\mathbf{E}(\mathbf{r},t)\, e^{-i\omega_i t}\, e^{i\mathbf{q}\cdot\mathbf{r}}d^3q$$

As a sanity test, we see that if the scattered wave varies as $e^{i\omega t}$, then $\chi(t)$ from Eq. D54 varies as $e^{i(\omega-\omega_i)t}$, as it should. When ω and ω_i are the same, then **k=k$_i$** and χ is independent of t and Eq. D54 reduces to the first Born expression for time-independent case.
We shall now return to Eq. D52 and calculate it without Born approximation.

$$\begin{aligned}\mathbf{E}_S(\mathbf{r},t) &= \frac{k^2}{4\pi}\frac{e^{ikr}}{r}\int d^3r'\, e^{-ik\cdot r'}\chi\left(r',t-\frac{r}{c}\right)\mathbf{E}_i(\mathbf{r}',t) \\ &\quad+\frac{k^2}{4\pi}\frac{e^{ikr}}{r}\int d^3r'\, e^{-ik\cdot r'}\chi\left(r',t-\frac{r}{c}\right)\mathbf{E}_S(\mathbf{r}',t) \\ &= \frac{k^2}{4\pi}\frac{e^{ikr}}{r}e^{i\omega_i t}\int d^3r'\,\chi\left(\mathbf{r}',t-\frac{r}{c}\right)e^{-i\mathbf{q}\cdot\mathbf{r}'} \\ &\quad+\frac{k^2}{4\pi}\frac{e^{ikr}}{r}\int d^3r'\, e^{-ik\cdot r'}\chi\left(r',t-\frac{r}{c}\right)\frac{e^{ikr'}}{r'}\mathbf{E}_S(\theta',\varphi',t)\end{aligned} \tag{D55}$$

In the extended far-field approximation (similar to D26 for frequency dependence) given by

$$\mathbf{E}_S(\theta',\phi',t) = \mathbf{E}_S(\theta,\phi,t) \tag{D56}$$

Substituting Eq. D56 in Eq. D55 and regrouping the terms we get,

$$\begin{aligned}\mathbf{E}_S(\mathbf{r},t) &= \frac{k^2}{4\pi}\frac{e^{ikr}}{r}e^{i\omega_i t}\int d^3r'\,\chi\left(\mathbf{r}',t-\frac{r}{c}\right)e^{-i\mathbf{q}\cdot\mathbf{r}'} \\ &\quad+\frac{k^2}{4\pi}\mathbf{E}_S(r,t)\int d^3r'\, e^{-ik\cdot r'}\chi\left(r',t-\frac{r}{c}\right)\frac{e^{ikr'}}{r'}\end{aligned} \tag{D57}$$

and collecting the like terms, Eq. D57 simplifies to

$$\mathbf{E}_S(\mathbf{r},t) = \frac{\frac{k^2}{4\pi}\frac{e^{ikr}}{r}e^{i\omega_i t}\int d^3r'\,\chi\left(\mathbf{r}',t-\frac{r}{c}\right)e^{-i\mathbf{q}\cdot\mathbf{r}'}}{1-\frac{k^2}{4\pi}\int d^3r'\, e^{-ik\cdot r'}\chi\left(r',t-\frac{r}{c}\right)\frac{e^{ikr'}}{r'}} \tag{D58}$$

The Eq. D58 can be inverted to obtain $\chi(r,t)$ in terms of $E_s(r,t)$ following the steps described in Eq. B6 to B11 in Appendix B.

APPENDIX E:
INELASTIC SCATTERING IN 2D

The equations derived in previous appendices are valid also for two dimensions with appropriate changes to spatial integration and the expression for the Green's function (GF). In two dimensions, the inelastically scattered field in the far field approximation using GF is:

$$E_s(\mathbf{r},\omega_s) = k_s^2 \frac{e^{i(k_s r+\pi/4)}}{\sqrt{8\pi k_s r}} \int d^2r' \, e^{-i\mathbf{k}_s\cdot\mathbf{r}'} \int d\omega' \, \chi(\omega_s-\omega')[E_i(\mathbf{r}',\omega')+E_s(\mathbf{r}',\omega')]\,. \qquad \text{(E1)}$$

Performing the integral over frequency, we obtain:

$$E_s(\mathbf{r},\omega_s) = k_s^2 \frac{e^{i(k_s r+\pi/4)}}{\sqrt{8\pi k_s r}} \int d^2r' \, e^{-i\mathbf{k}_s\cdot\mathbf{r}'} [\chi(\omega_s-\omega_i)E_i(\mathbf{r}',\omega_i)+\chi(0)E_s(\mathbf{r}',\omega_s)]\,. \qquad \text{(E2)}$$

Assuming a monochromatic incident wave of the form $E_i(\mathbf{r}',\omega_i) = e^{i\mathbf{k}_i\cdot\mathbf{r}'}$, Eq. (E2) becomes:

$$E_s(\mathbf{r},\omega_s) = -k_s^2 \frac{e^{i(k_s r+\pi/4)}}{\sqrt{8\pi k_s r}} \Big[\chi(\omega_s-\omega_i)\int d^2r' \, e^{-i\mathbf{q}\cdot\mathbf{r}'} + \chi(0)\int d^2r' \, e^{-i\mathbf{k}_s\cdot\mathbf{r}'} E_s(\mathbf{r}',\omega_s)\Big], \qquad \text{(E3)}$$

where $\mathbf{q} \equiv \mathbf{k}_s - \mathbf{k}_i$. Defining the scattering amplitude as:

$$f(\mathbf{k}_s,\mathbf{k}_i) \equiv E_s(\mathbf{r},\omega_s)\frac{\sqrt{8\pi k_s r}}{e^{i(k_s r+\pi/4)}} \qquad \text{(E4)}$$

and applying the EFA to the scattered field within the object,

$$E_s(\mathbf{r}',\omega_s) = \frac{e^{i(k_s r'+\pi/4)}}{\sqrt{8\pi k_s r'}} f(\mathbf{k}_s,\mathbf{k}_i)\,, \qquad \text{(E5)}$$

Eq. (E3) can be written as:

$$f(\mathbf{k}_s,\mathbf{k}_i) = -k_s^2\left[\chi(\omega_s-\omega_i)\int d^2r' \, e^{-i\mathbf{q}\cdot\mathbf{r}'} + \chi(0) f(\mathbf{k}_s,\mathbf{k}_i)\int d^2r' \, e^{-i\mathbf{k}_s\cdot\mathbf{r}'} \frac{e^{i(k_s r'+\pi/4)}}{\sqrt{8\pi k_s r'}}\right]. \qquad \text{(E6)}$$

Solving for the scattering amplitude, we obtain:

$$f(\mathbf{k}_s,\mathbf{k}_i) = \frac{-k_s^2\chi(\omega_s-\omega_i)\int d^2r' \, e^{-i\mathbf{q}\cdot\mathbf{r}'}}{1+k_s^2\chi(0)\int d^2r' \, e^{-i\mathbf{k}_s\cdot\mathbf{r}'} \dfrac{e^{i(k_s r'+\pi/4)}}{\sqrt{8\pi k_s r'}}} \qquad \text{(E7)}$$

The integral in the numerator of Eq. (E7) can be evaluated in cylindrical coordinates as:

$$\begin{aligned}\int d^2r' \, e^{-i\mathbf{q}\cdot\mathbf{r}'} &= \int_0^a dr' \, r' \int_0^{2\pi} d\theta e^{-iqr'\cos\theta} \\ &= \int_0^a dr' \, r' \, 2\pi J_0(qr') \\ &= \frac{2\pi a}{q} J_1(qa)\end{aligned} \qquad \text{(E8)}$$

where $J_i(x)$ are Bessel functions. The integral in the denominator of Eq. (E7) cannot be solved analytically, but it can be reduced to the following form:

$$\int d^2r' e^{-i\mathbf{k}_s\cdot\mathbf{r}'}\frac{e^{i(k_s r'+\pi/4)}}{\sqrt{8\pi k_s r'}} = \int_0^a dr' r' \frac{e^{i(k_s r'+\pi/4)}}{\sqrt{8\pi k_s r'}}\int_0^{2\pi} d\theta e^{-ik_s r'\cos\theta}$$
$$= \int_0^a dr' r' \frac{e^{i(k_s r'+\pi/4)}}{\sqrt{8\pi k_s r'}} 2\pi J_0(k_s r') \tag{E9}$$

Thus, the final expression for the scattering amplitude is:

$$f(\mathbf{k}_s,\mathbf{k}_i) = \frac{-k_s^2\chi(\omega_s-\omega_i)\frac{2\pi a}{q}J_1(qa)}{1+2\pi k_s^2\chi(0)\int_0^a dr' r' \frac{e^{i(k_s r'+\pi/4)}}{\sqrt{8\pi k_s r'}}J_0(k_s r')}. \tag{E10}$$